Supplement of Atmos. Chem. Phys., 20, 6973–6990, 2020
https://doi.org/10.5194/acp-20-6973-2020-supplement

Supplement of

MAX-DOAS measurements of NO_2, SO_2, HCHO, and BrO at the Mt. Waliguan WMO GAW global baseline station in the Tibetan Plateau

Jianzhong Ma et al.

Correspondence to: Thomas Wagner (thomas.wagner@mpic.de) and Jianzhong Ma (majz@cma.gov.cn)

S1 Meteorological conditions

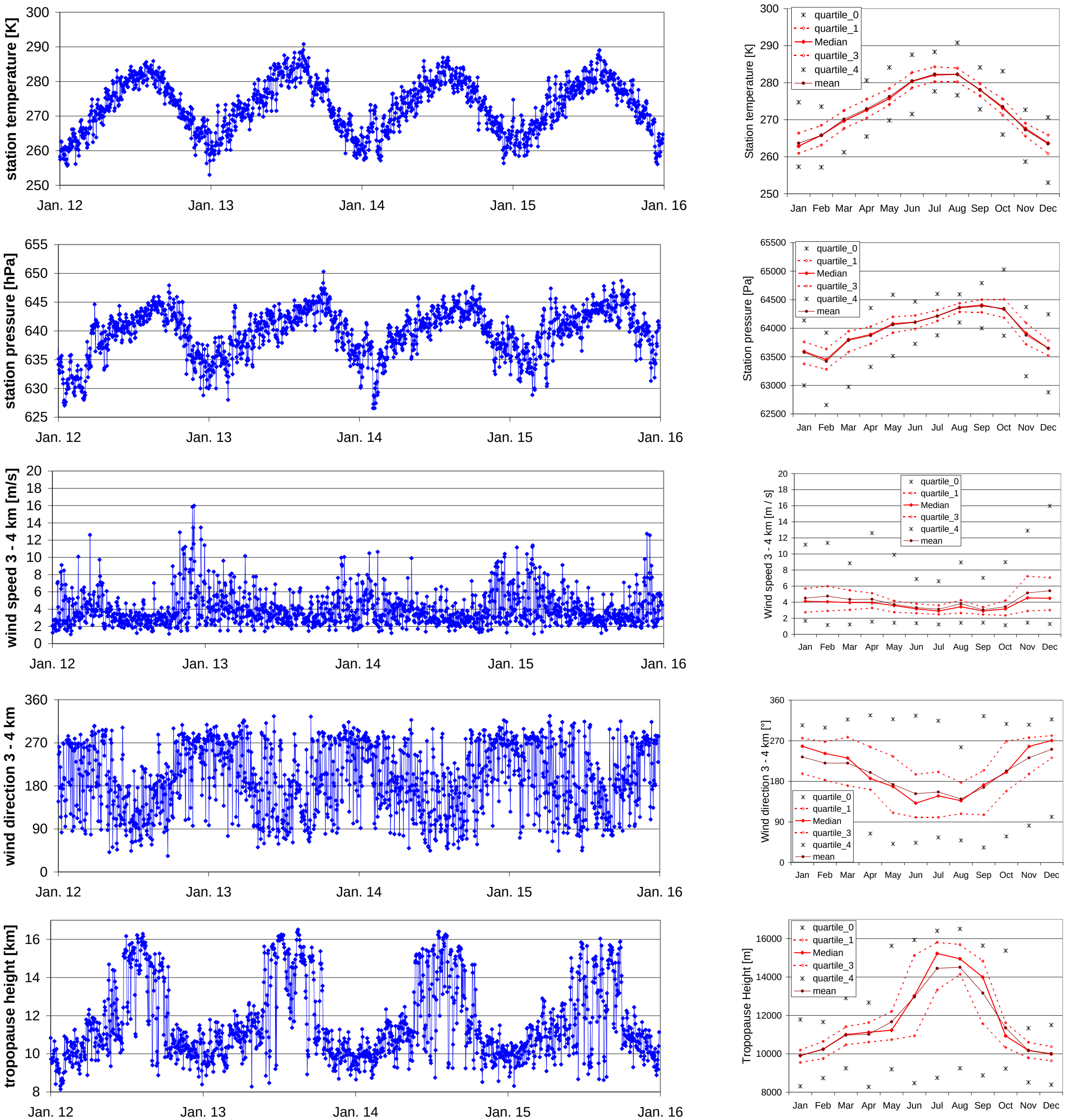

Fig. S1 Left: Time series of daily averaged values of different meteorological quantities at WLG station derived from ECMWF data (2012 to 2015), with ‘Jan 12’ referring to ‘1 Jan 2012’. **Right:** The corresponding seasonal cycles.

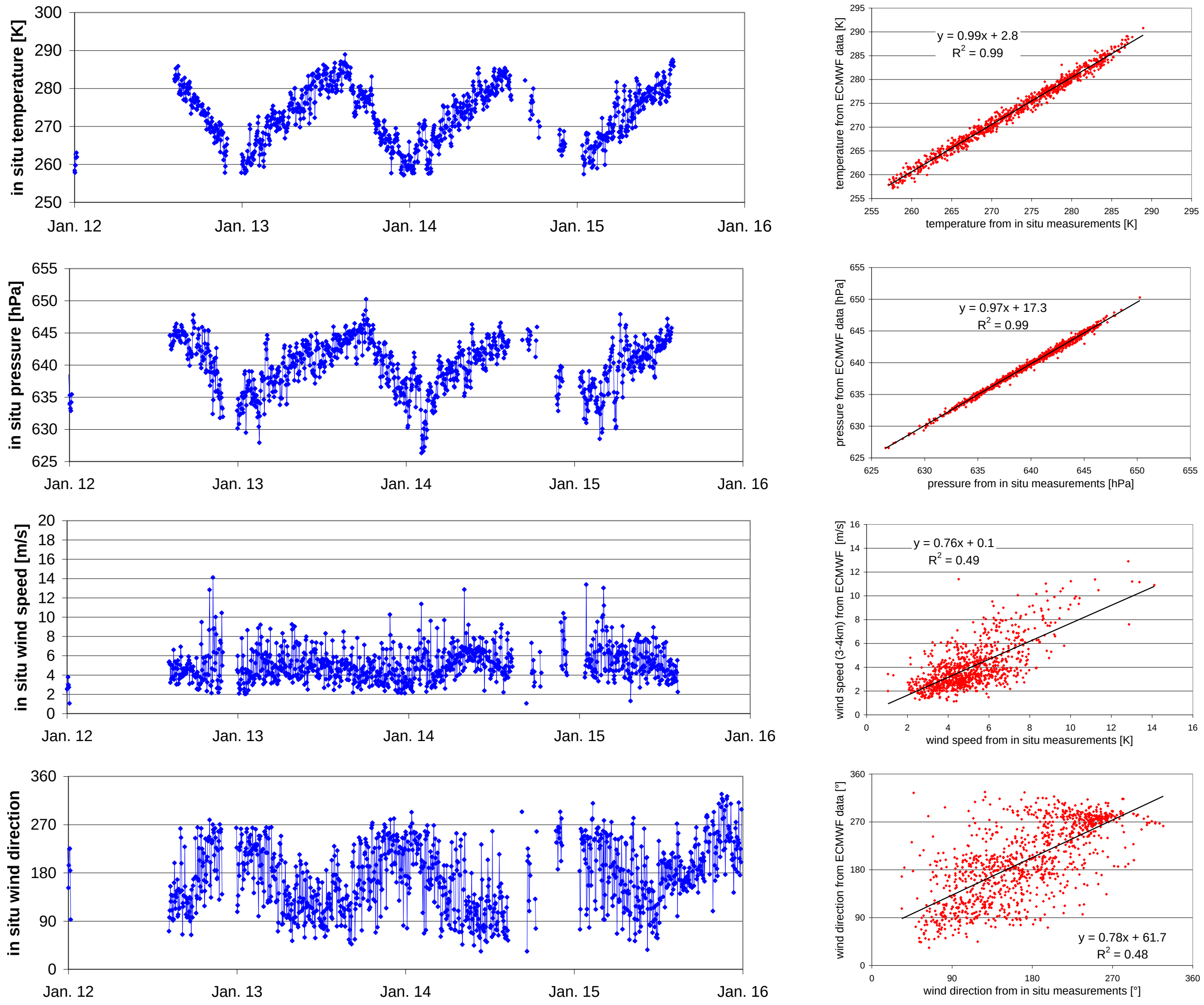

Fig. S2 Left: Time series of daily averaged meteorological data from the in situ measurements at WLG (2012 to 2015) , with 'Jan 12' referring to '1 Jan 2012'.. **Right:** Correlation plots of the ECMWF versus the corresponding in situ data.

S2 Determination and correction of the elevation calibration

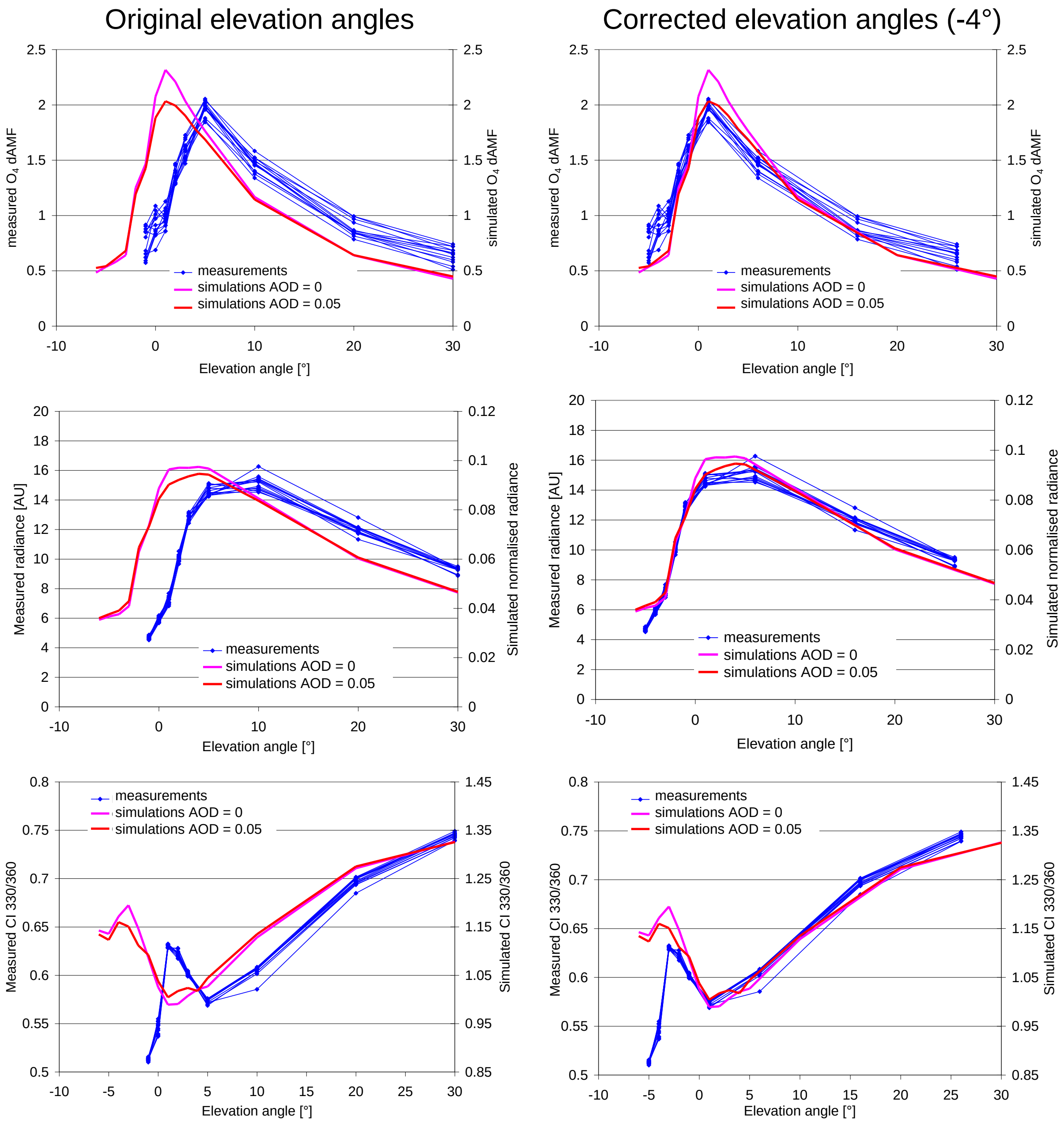

Fig. S3 Comparison of simulated (magenta and red lines) and measured (blue lines) O_4 absorption (expressed as O_4 air mass factor), radiance at 360 nm, and colour index (CI) for 330 and 360 nm. For the comparison, measurements around noon on a clear day (14.04.2013) were selected. Simulations were made for two different aerosol loads (magenta: no aerosols, red: AOD = 0.05). The SZA is about 30°, and the relative azimuth angle is about 180°. **Left:** measurements are displayed as function of the original (wrong) elevation angle calibration. **Right:** The figures show the same data, but with the measurements as function of the corrected (by -4°) elevation angles.

S3 Spectral retrieval

Table S1. Selected periods with different (stable) detector temperatures, which were selected for the data analysis

Period	**Number of days**
01.04.2012 – 30.06.2012	~60 days
19.07.2012 – 02.12.2012	~130 days
02.12.2012 – 24.06.2013	~200 days
24.06.2013 – 21.11.2013	~150 days
22.11.2013 – 07.03.2014	~100 days
02.04.2014 – 20.05.2014	~50 days
20.05.2014 – 01.10.2014	~130 days
17.10.2014 – 04.04.2015	~170 days
Total	
01.04.2012 – 04.04.2015	~990 days

S3.1 Averaging of individual spectra

Averaging of spectra increases the signal to noise ratio and thus reduces the statistical error of the spectral retrieval. In order to achieve a large reduction of the statistical error, as much as possible individual spectra should be averaged. However, besides the statistical errors also systematic errors occur, e.g. caused by imperfect correction of the Ring effect or different saturation levels of the detector. Such systematic errors tend to increase if an increasing number of spectra are averaged, because the solar zenith angle (and other atmospheric or instrumental properties) changes during the selected period. Thus it is important to find an ‘optimum number’ of individual spectra for the averaging, for which a minimum of the fit error is found.

In Fig. S4 the effect of averaging of different numbers of spectra on the RMS of the spectral analysis is shown. The analysis of spectra averaged from 10 original spectra leads to a strong reduction of the RMS (decreases by a factor of 2 to 3.5) compared to the results for individual spectra, indicating that for individual spectra the total error is dominated by noise. However, further averaging of spectra (40 original spectra) only leads to a rather small improvement of the RMS. Thus in this study, averages of 10 original spectra are analysed.

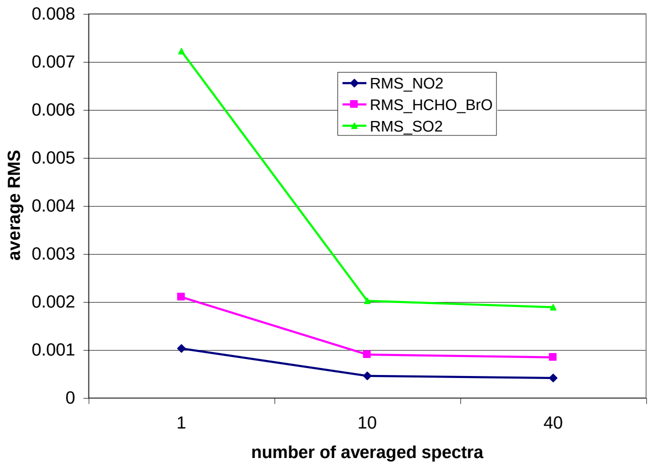

Fig. S4 Mean RMS of the NO_2, SO_2, and HCHO and BrO analysis for spectra taken at 1°, 6°, and 16° elevation for clear sky measurements in April 2013 as function of the number of averaged spectra.

S3.2 Choice of Fraunhofer reference spectra

Usually, spectra at high elevation angle (usually 90°) and low solar zenith angle (SZA) are used as a Fraunhofer reference spectrum, because such measurements in general contain the smallest atmospheric absorptions. Such a choice was also first used for the analysis of the WLG measurements. However, it turned out that for zenith spectra larger fit errors occurred than for the spectra at low elevation angles (see Fig. S5 (right)). Moreover, also unreasonable results were obtained for the trace gas absorptions and the Ring effect (see Fig. S5 (left)). The main reason for the problems of the zenith spectra is probably that no black tube was mounted in front of the telescope lense. Thus direct sun light can fall on the telescope lense when the instrument points to zenith (since the instrument is directed towards the North, no direct sun light falls on the telescope for the low elevation angles). Part of the direct sun light will be scattered by the lense onto the fibre bundle and will be added to the ‘regular’ scattered sun light. If the lense is covered by dirt, the contribution of the direct sun light might be further increased. Here it should be noted that at the high altitude of the measurement site the contribution of direct sun light is substantially enhanced compared to measurements at sea level, because of the reduced molecular scattering in the atmosphere above the instrument.

The effect of the direct sun light is (at least) twofold:

1) the probability of Raman scattering (Ring effect) will be changed. Thus the correction of the Ring effect will work less good as for spectra of purely scattered sunlight, and spectral interferences with trace gas absorptions might appear. Here it is important to note that unrealistic values for 90° measurements were not only found for the Ring effect, but also for the absorptions of NO_2 SO_2, HCHO, and BrO.

2) the broad band spectral shape of the spectra changes, the spectra become more ‘reddish’. Thus spectrograph straylight will probably be enhanced compared to spectra or purely scattered sun light. Indeed, a much higher variation of the fitted intensity offset is found for spectra in 90° elevation than for the other elevation angles.

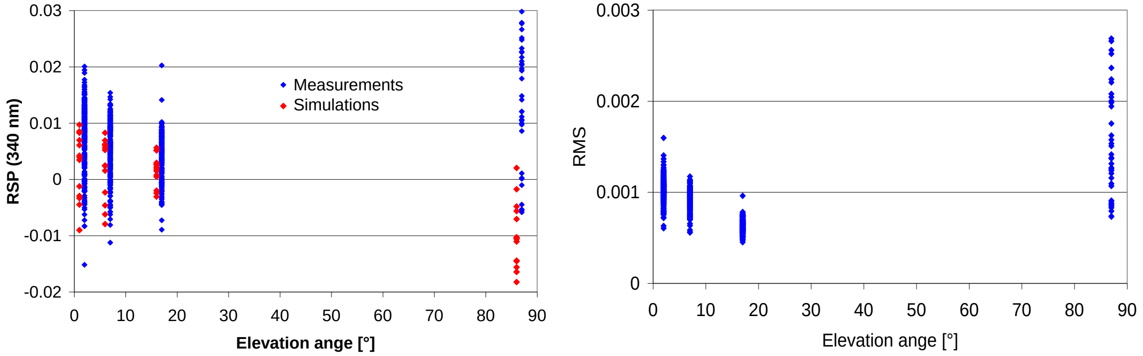

Fig. S5 Left: Results for the Ring effect (expressed as Raman scattering probability, RSP) as function of the elevation angle for measurements from 02 December 2012 to 24 June 2013 (blue) and derived from radiative transfer simulations (red). **Right:** RMS of the spectral fit for BrO and HCHO as function of the elevation angle for measurements from 02 December 2012 to 24 June 2013. The measurements were analyzed using Fraunhofer reference spectra taken at 26 °of each elevation sequence.

In Fig, S5 (left) the measured Ring effect (expressed as Raman scattering probability, RSP) is compared to simulation results of a radiative transfer model. The measurements were analysed using individual Fraunhofer reference spectra taken at 26 ° elevation of each elevation sequence. Accordingly, also for the simulated RSP values, the corresponding results for 26 ° elevation were subtracted. The simulations were performed for SZA between 20 ° and 60 ° and relative azimuth angles between 60 ° and 180 °, which corresponds to the variation of both quantities for the selected measurements (02 December 2012 to 24 June 2013). The rather large scatter of the measured and simulated RSP values is mainly caused by the variations of these two quantities. In spite of the rather large scatter, still a large discrepancy between the measured and simulated RSP values is found for 90 ° elevation, while for the low elevation angles, the agreement is much better. Because of these findings, in this study no measurements at 90 ° elevation are used as Fraunhofer reference spectra. Instead, individual measurements at 26 ° elevation of each elevation sequence are used as Fraunhofer reference spectra.

S3.3 Choice of spectral ranges for the different spectral analyses

Table S2a Fit settings for the NO_2 spectral analyses.

NO_2 analysis	
Wavelength range (nm)	399 – 426
DOAS polynomial	degree: 4
Intensity offset	degree: 2
Gaps (nm)	422.4 – 423.1
Ring effect	Original and wavelength-dependent Ring spectrum
NO_2	220 K, Vandaele et al. (2002)
O_3	223 K, Io corrected, Bogumil et al. (2003)
RMS filter	5e-4

Table S2b Fit settings for the SO_2 spectral analyses.

SO_2 analysis	
Wavelength range (nm)	306 – 325
DOAS polynomial	degree: 6
Intensity offset	degree: 2
Gaps (nm)	-
Ring effect	Original and wavelength-dependent Ring spectrum
SO_2	273 K, Bogumil et al. (2003)
NO_2	220 K, Vandaele et al. (2002)
O_3	223 K, Io corrected, Bogumil et al. (2003)
O_3, wavelength dependent	O_3 cross section multiplied with wavelength, orthogonalised to original O_3 cross section
RMS filter	1.8e-3

Table S2c Fit settings for the BrO/HCHO spectral analyses.

BrO / HCHO analysis	
Wavelength range (nm)	314 – 358
DOAS polynomial	degree: 8
Intensity offset	degree: 2
Gaps (nm)	331.4 – 331.6, 336.4 – 336.8, 349.0 – 349.3
Ring effect	Original and wavelength-dependent Ring spectrum
BrO	228K, Wilmouth et al. (1999)
HCHO	298K, Meller and Moortgat (2000)
NO_2	220 K, Vandaele et al. (2002)
O_4	293 K, Thalman and Volkamer (2013)*
O_3	223 K, Io corrected, Bogumil et al. (2003)
RMS filter	9e-4

*It should be noted that in addition to the original cross section also a modified cross section including the O_4 absorption band at 328 nm was tested (see Lampel et al., 2018)). It was found that the BrO and HCHO dSCDs retrieved using the modified O_4 cross section were almost identical (deviations < 2%) with the results from the analysis with the original cross section.

Table S2d Fit settings for the O_4 spectral analyses.

O_4 analysis	
Wavelength range (nm)	352 – 387
DOAS polynomial	degree: 5
Intensity offset	degree: 2
Gaps (nm)	-
Ring effect	Original and wavelength-dependent Ring spectrum
O_4	293 K, Thalman and Volkamer (2013)
NO_2	220 K, Vandaele et al. (2002)
O_3	223 K, Io corrected, Bogumil et al. (2003)

S3.3.1 Determination of the optimum fit range for HCHO and BrO

For this task both synthetic and measured spectra are used. Different tests are performed to find the best suited fit range for both species. The results are summarized in Table S3 below. Based on these results, a fit range from 314 to 358 nm was chosen. The individual tests are described in more detail below.

Table S3 Best fit ranges based on different test results.

Test	**Optimum lower fit limit for HCHO (nm)**	**Optimum upper fit limit for HCHO (nm)**	**Optimum lower fit limit for BrO (nm)**	**Optimum upper fit limit for BrO (nm)**
Comparison with input values of synthetic spectra	313 – 314	356 – 360	314 – 316	356 – 360
Consistency between synthetic and measured spectra	314 - 316	358 – 359	314 – 316	357 – 358
Fit error (in brackets: results for synthetic spectra)	312 – 317	358	312 – 318 (312 – 316)	357 – 358 (358 – 360)
RMS (in brackets: results for synthetic spectra)	316 – 318 (314 – 318)	356 – 358 (356 – 360)	316 – 318 (314 – 318)	356 – 358 (356 – 360)
scatter of results for 1° elevation angle (in brackets: results for synthetic spectra)	316 (312 – 317)	358 – 360 (356 – 358)	315 – 316 (312 – 313)	358 – 360 (358 – 360)
correlation between BrO and HCHO dSCDs for 1° elevation angle (in brackets: results for synthetic spectra)	312 – 313 (313 – 318)	358 – 360 (312 – 313)	312 – 313 (313 – 318)	358 – 360 (312 – 313)
Final selection	**314**	**358**	**314**	**358**

Synthetic spectra

Synthetic spectra were simulated at high spectral resolution for the spectral range 303 – 390 nm using the RTM SCIATRAN. Rotational Raman scattering was included. The simulations were performed for a SZA of 50° and a relative azimuth angle (RAA) of 180°. Surface albedo and altitude were set to 0.07 and 3800m, respectively.

An aerosol layer between 3800 and 4800m with an AOD of 0.1 was assumed. The single scattering albedo and phase function were chosen according to biomass burning aerosols. For the ozone absorption the temperature dependence was taken into account. Information about the chosen trace gas cross sections and assumed atmospheric profiles is given in Table S4.

The Radiance output is convoluted with a Gaussian function with FWHM of 0.6 nm. Random noise with a RMS of 5e-4 is added to the convoluted spectra. 100 spectra with different noise are simulated for each elevation angle.

In addition to the simulated spectra, also air mass factors are derived from the RTM for the following wavelengths: 315, 340, 355 nm. The resulting dSCDs for BrO and HCHO are shown in Fig. S6. The dSCDs are calculated assuming a Fraunhofer reference spectrum measured at 26 ° elevation angle. The dSCDs derived in this way are compared to the results of the spectral analyses. For this comparison, the analysis results of the 100 spectra for each elevation angle are averaged. For BrO and HCHO the dSCDs calculated for 340 nm are used for the comparison.

Table S4 Trace gas cross sections and atmospheric profiles used for the synthetic spectra

Trace gas	Cross section	Atmospheric profile
NO_2	NO2_vandaele97_220_vac.txt	Box profile in the lowest 0.5km. VCD: 1e15 molec/cm²; stratospheric profile with maximum at 24 km. VCD: 5.22e15 molec/cm²
HCHO	HCHO_Meller_298_vac.DAT	Box profile in the lowest 1km. VCD: 1e15 molec/cm²
BrO	bro_wil_228_vac.txt	stratospheric profile with maximum at 20 km. VCD: 3e13 molec/cm²
O_3	O3_203K_V3_0.dat O3_223K_V3_0.dat O3_243K_V3_0.dat O3_273K_V3_0.dat O3_293K_V3_0.dat	From the US standard atmosphere: maximum at 22km. VCD: 9.03e18 molec/cm² (337 DU)
O_4	o4_thalman_volkamer_293K_corr.xs	O_4 derived from temperature and pressure profile

Interestingly, different elevation dependencies are found for both trace gases (Fig. S6). For BrO, the dSCDs decrease towards low elevation angles. This is caused by the fact that in the RTM simulations BrO is only located in the stratosphere. Measurements at 26 ° elevation (Fraunhofer reference spectra) are more sensitive to these altitudes than measurements at low elevation angles. Thus, for low elevation angles, negative BrO dSCDs are obtained. For HCHO, the opposite elevation dependence is found, because HCHO is only located in the troposphere.

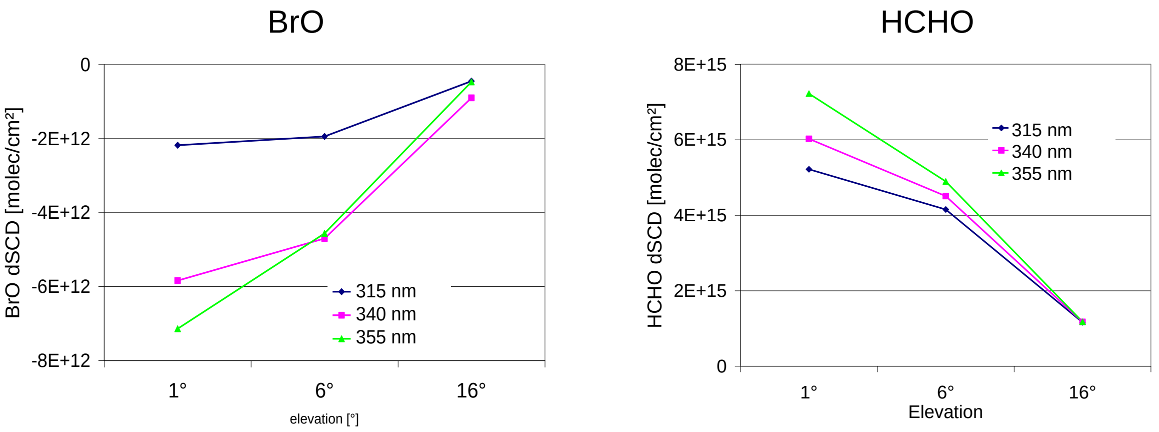

Fig. S6 Dependence of the simulated trace gas dSCDs for BrO (**left**) and HCHO (**right**) on the elevation angle for different wavelengths used for the AMF calculations.

Measured spectra

Measurements for the period 02.12.2012 – 24.06.2013 were selected. This period covers ~200 days in different seasons. For the analysis of the measured spectra the same settings as for the synthetic spectra were used. Only measurements for clear sky and with scan numbers > 800 were considered.

Dependence of the retrieved BrO and HCHO dSCDs on the upper and lower fit boundaries

Figure S7 shows results for 1 ° elevation angle (similar results are found for the other elevation angles). In addition to the results for the measured spectra (red lines), the results for the synthetic spectra (blue lines) together with the 'true dSCDs' (blue dashed lines) are shown.

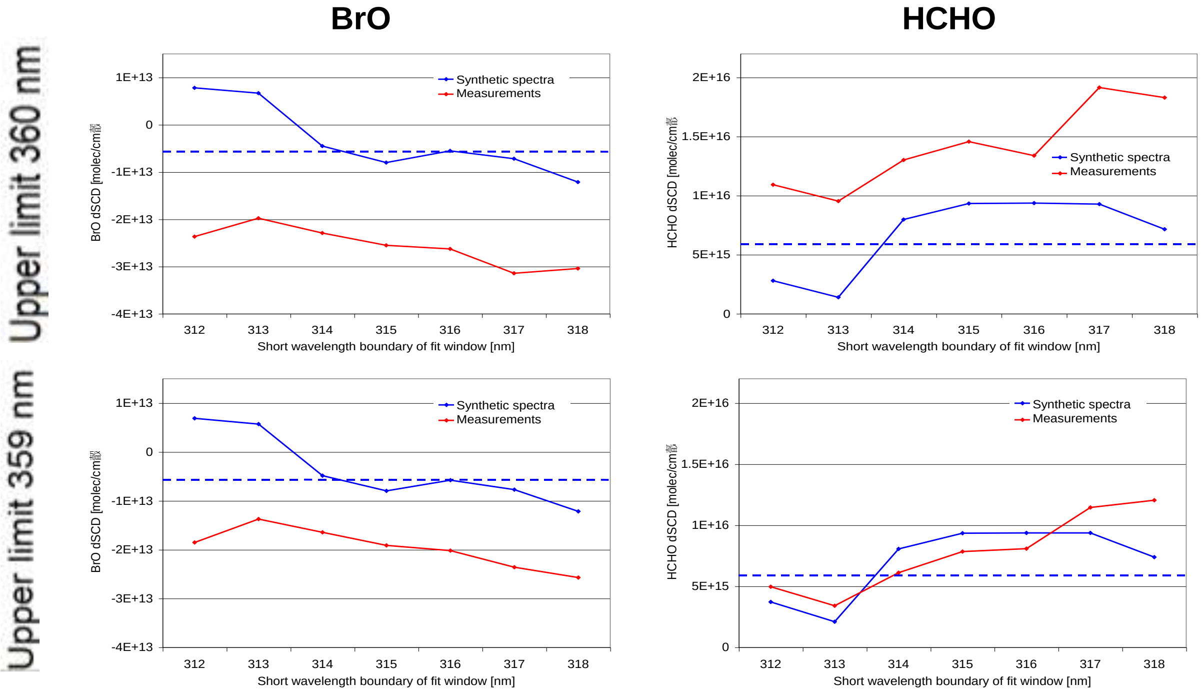

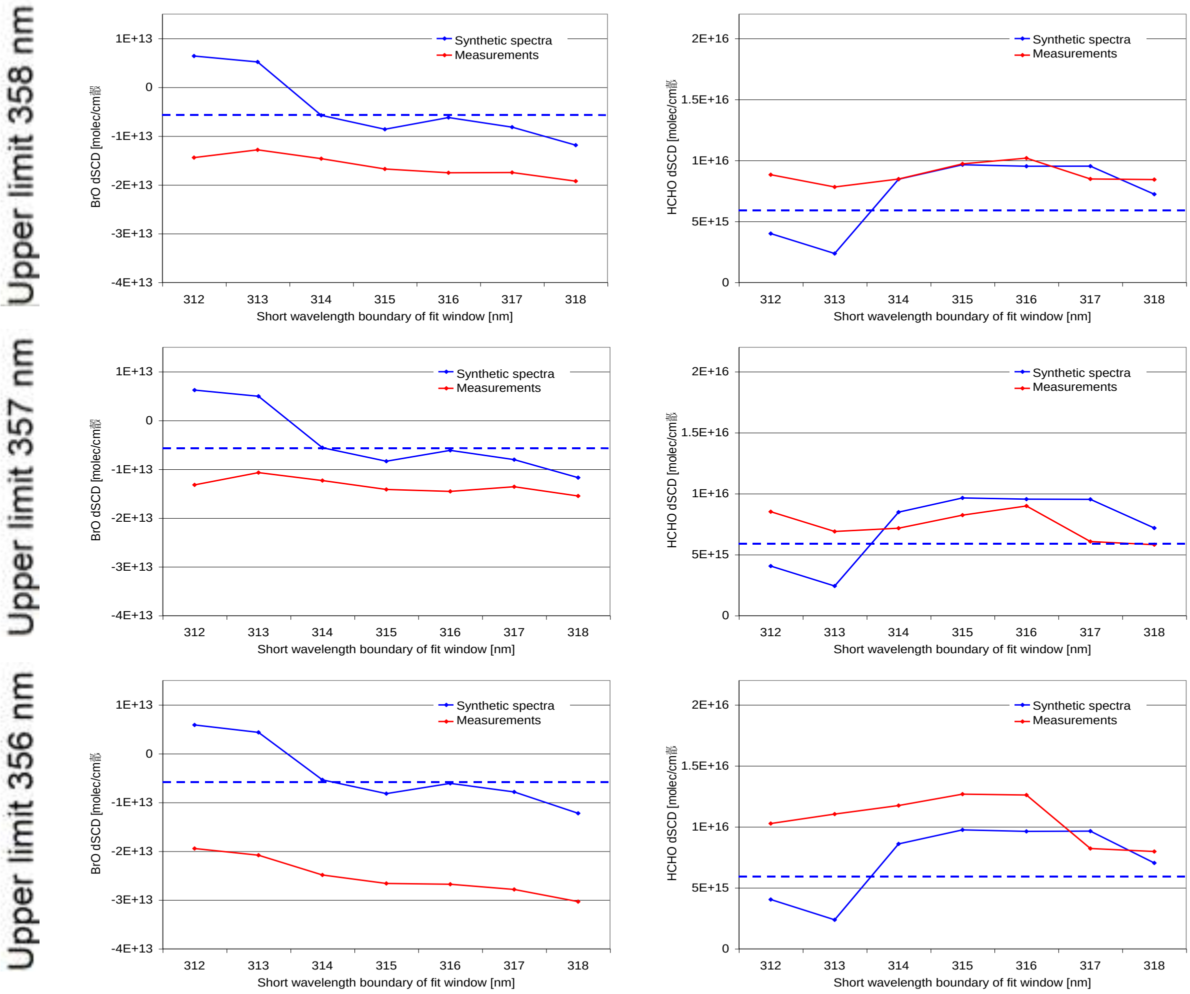

Fig. S7 Dependence of the fit results (at 1 ° elevation angle) for the measured spectra (red lines) and synthetic spectra (blue lines) on the upper and lower boundaries of the fit range. Also shown are the 'true dSCDs' derived from the simulated air mass factors (blue dashed lines). The individual plots represent results for one fixed upper wavelength limit. The lower wavelength limit is represented by the x-axes.

The individual figures show the results for one value of the upper limit of the fit range. The x-axes indicate the lower limit of the fit range. For the comparison of the results for measured and synthetic spectra it has to be taken into account that the true atmospheric profiles are not known. They might especially differ from the profiles assumed for the simulation of the synthetic spectra. Thus no perfect quantitative agreement can be expected. However, it is meaningful to compare the overall dependencies on the upper and lower limits of the fit ranges. Here quite good agreement is found (except for the lowest values for the lower fit boundary) indicating that the results for the synthetic spectra are well representative also for the measured spectra. For BrO the best agreement between the results of the synthetic spectra and the 'true dSCDs' is found for lower limits between 314 and 316 nm, while for the upper limits no clear dependency is found. For HCHO the best agreement between the results of the synthetic spectra and the ‘true dSCDs’ is found for lower limits between 313 and 316 nm. Again, for the upper limits no clear dependency is found.

Fit error and RMS

The errors of the BrO and HCHO dSCDs and RMS values derived from the fit are investigated for the measured and synthetic spectra. While for a fixed wavelength range, an increasing RMS is usually also accompanied by an increasing fit error, both quantities might depend differently on the variation of the fit boundaries. Fig. S8 shows the fit errors and RMS for synthetic (left) and measured spectra (right). In general, systematically higher fit errors and RMS are found for the measured spectra. This probably indicates higher noise levels, but also additional systematic errors, caused e.g. by imperfect convolution, errors of the input cross sections, or remaining temperature dependencies.

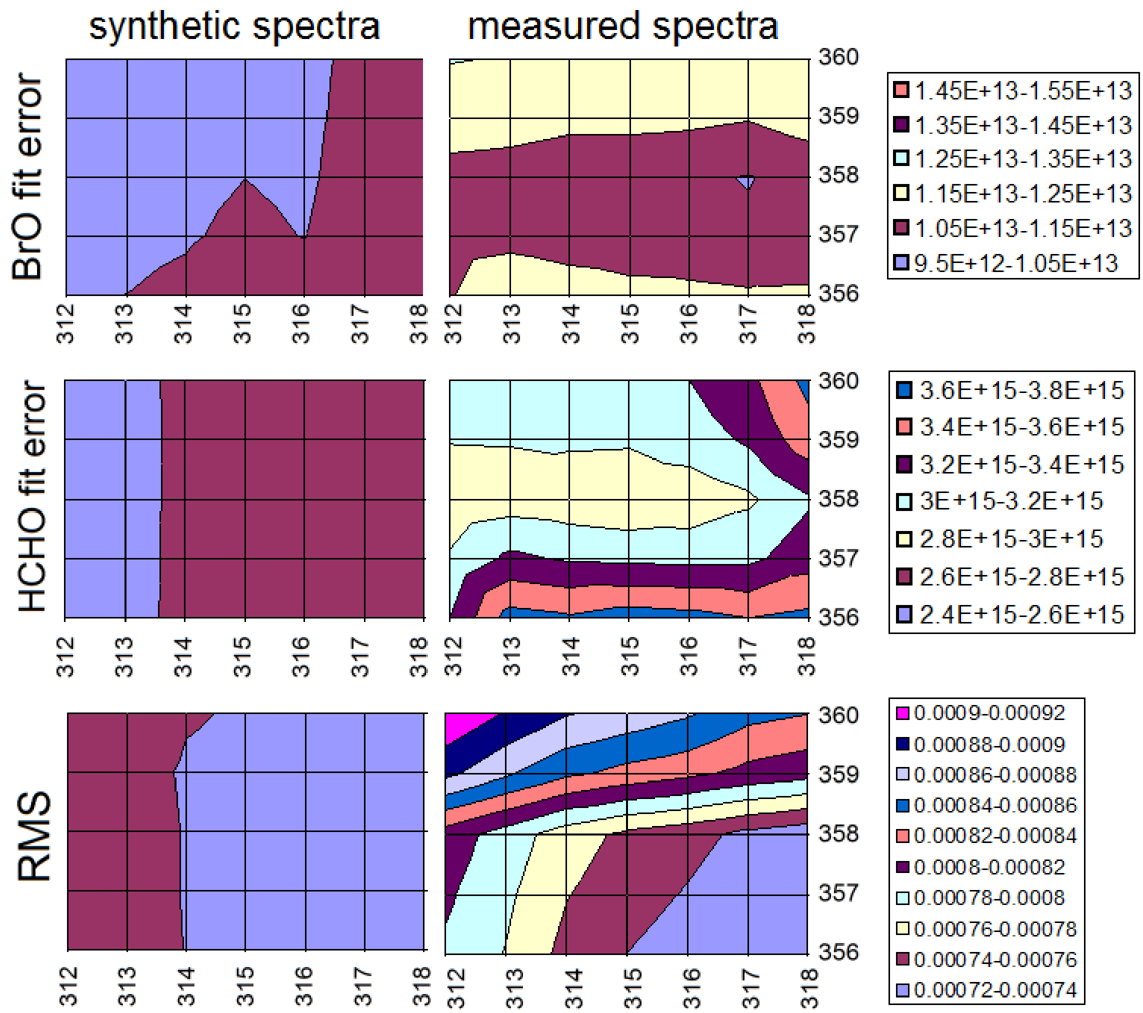

Fig. S8 Dependence of the fit errors and RMS on the upper and lower boundaries of the fit range for the synthetic **(left)** and measured spectra **(right)**.

Standard deviation of the retrieved dSCDs and correlation between the dSCDs of BrO and HCHO

In this section, the temporal variability of the fit results is investigated. For this task, the results for 1 ° elevation are chosen, because they are expected to show the highest trace gas dSCDs and the largest variability. Since for the synthetic spectra the same input profiles are used for all spectra, the same trace gas dSCDs should be retrieved. Moreover, no correlation between the dSCDs of BrO and HCHO is expected. However, since noise was added to the synthetic spectra, also the derived trace gas dSCDs might be affected by some random variation, leading eventually also to some correlation between the dSCDs of BrO and HCHO.

For the measurements, also the atmospheric trace gas concentrations can vary. Moreover, also changes of the atmospheric visibility will probably contribute to a variation of the measured trace gas dSCDs. Thus the retrieved variability of the trace gas dSCDs for the measured spectra is expected to be higher than for the synthetic dSCDs. For the measured spectra, a (anti-) correlation of the derived dSCDs of BrO and HCHO might reflect a (anti-) correlation of their true atmospheric absorptions. However, such a (anti-) correlation is not very probable because of the rather different atmospheric profile shapes and formation processes. Thus a low correlation between the dSCDs of BrO and HCHO is considered as an indication for a good fit quality for both the synthetic and measured spectra.

Figure S9 shows the standard deviation of the time series of the dSCDs of BrO and HCHO for 1 ° elevation angle as well as the correlation coefficient between both dSCDs for the synthetic (left) and measured spectra (right). As expected the standard deviations are higher for the measured spectra. Also the correlation between both species is higher for the measured spectra. This finding might partly represent a true correlation of the atmospheric abundances, but is more probably caused by the noise of the spectra.

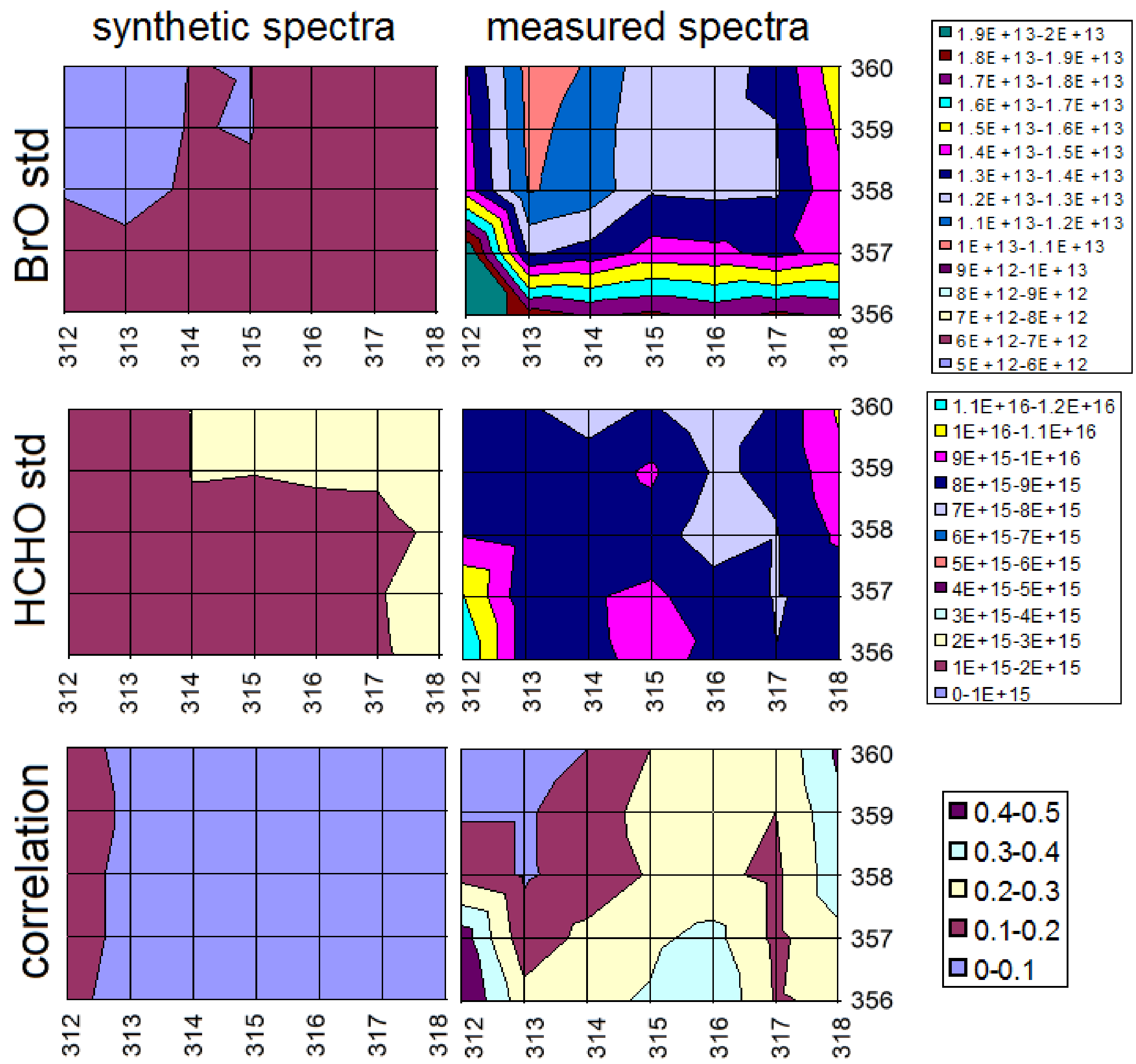

Fig. S9 Dependence of the variation (expressed as standard deviation) of the fit results for 1 ° elevation angle and the correlation between the BrO and HCHO dSCDs (expressed as r^2) on the upper and lower boundaries of the fit range. For the synthetic **(left)** and measured spectra **(right)**.

Final choice of fit the range

Based on the results from the previous sub-section, the fit range from 314 to 358 nm is chosen for the analysis of BrO and HCHO. This choice is mainly based on the results of the comparison of the retrieved trace gas dSCDS derived from the synthetic spectra to the dSCDs derived from the measured spectra and the 'true dSCDs'. For the chosen fit range, also the fit errors, the standard deviation of the dSCDs (for 1 ° elevation), and the correlation between the dSCDs of BrO and HCHO are rather small.

Error estimate

The systematic and random uncertainties of the fit results for individual spectra (average of 10 original spectra) are summarized in Table S8.

Table S5 overview on the different systematic and random error sources

error source	**error of BrO fit result**	**error of BrO fit result**
systematic errors		
Comparison of the fit results for the synthetic spectra to the ‘true dSCDs’	3e12 molec/cm²	4e15 molec/cm²
random errors		
Fit error	1.1e13 molec/cm²	3e15 molec/cm²
Standard deviation*	1.1e13 molec/cm²	9e15 molec/cm²

*the standard deviation describes the total statistical error; at least part of the total statistical error is caused by the fit error.

The systematic error of the dSCDs is usually dominated by systematic effects of the spectral retrieval, which are quantified by the comparison of the fit results for the synthetic spectra to the ‘true dSCDs’. Only for high trace gas dSCDs the uncertainty of the cross section might become important. But for the rather low trace gas dSCDs retrieved in this study the uncertainty of the cross section can be neglected.

For individual measurements, the random errors clearly dominate the total uncertainty. However, if several measurements are averaged these errors can be largely reduced.

Quality filter

Spectra with bad fit quality have to be removed from further processing. First, measurements with a small number of individual scans (<800) are removed. This filter removes spectra with the worst fit results. In addition, a RMS filter is applied. Here a threshold for the RMS of 9e-4 is chosen. Figure S10 shows the frequency distribution of the RMS (for measurements with more than 800 scans). The RMS threshold removes about 24% of the BrO and HCHO results.

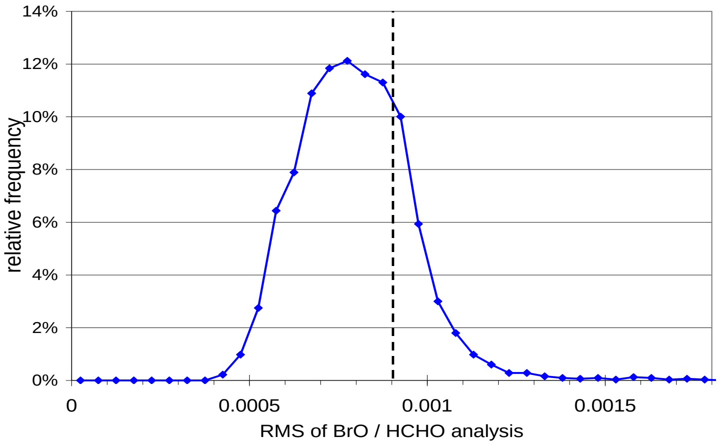

Fig. S10 frequency distribution of the RMS of the spectral analysis of BrO and HCHO for clear sky conditions. The vertical line indicates the threshold for removing measurements with high fit errors.

S3.3.2 Determination of the optimum fit range for SO_2

In this task both synthetic and measured spectra are used. Different tests are performed to find the best suited fit range for both species. The results are summarized in Table S6 below. Based on these results a fit range from 306 to 325 nm was chosen. The individual tests are described in more detail below.

Table S6 Best fit ranges based on different test results.

Test	**Optimum lower fit limit for SO_2 (nm)**	**Optimum upper fit limit for SO_2 (nm)**
Comparison with input values of synthetic spectra	304 – 308	323 – 327
Consistency between synthetic and measured spectra	306 – 307	323 – 327
Fit error (in brackets: results for synthetic spectra)	305 – 306 (304)	323 – 327 (323 – 327)
RMS (in brackets: results for synthetic spectra)	308 (304)	323 – 327 (323 – 327)
scatter of results for 1° elevation angle (in brackets: results for synthetic spectra)	306 – 307 (304)	323 – 327 (325 – 327)
correlation between BrO and HCHO dSCDs for 1° elevation angle (in brackets: results for synthetic spectra)	304 & 306 (308)	323 – 327 (325 – 327)
Final selection	**306**	**325**

Synthetic and measured spectra

The same data sets as for the BrO and HCHO analysis are used also for the determination of the fit range of SO_2 (see Supplement Sect. 3.3.3). Since no SO_2 absorptions are included in the simulation of the synthetic spectra, also the derived SO_2 dSCDs should be (close to) zero.

Dependence of the retrieved SO_2 dSCDs on the upper and lower fit boundaries

Figure S11 shows results for 1 °elevation angle (similar results are found for the other elevation angles). In addition to the results for the measured spectra (red lines), the results for the synthetic spectra (blue lines) together with the 'true dSCDs' (blue dashed lines) are shown. The individual figures show the results for one value of the upper limit of the fit range. The x-axes indicate the lower limit of the fit range. For the comparison between the results for measured and synthetic spectra it has to be taken into account that the true atmospheric profiles are not known. They might especially differ from the profiles assumed for the simulation of the synthetic spectra (zero SO_2 absorption). Thus no perfect quantitative agreement can be expected. And indeed, the derived SO_2 dSCDs from the measured spectra differ substantially (by up to 2e16 molec/cm^2) from those of the synthetic spectra. Also the dependence on the lower fit boundary is very different for measured and synthetic spectra. While the retrieved dSCDs for the synthetic spectra are close to zero, the retrieved dSCDs for the measured show as well negative as positive values. The differences of the results for synthetic and measured spectra indicate that the measurements are strongly influenced by factors like instrumental properties, which don’t affect the synthetic spectra. For both data sets, the smallest deviations from zero are found for lower fit boundaries of 306 and 307 nm. The choice of the upper fit boundary has almost no influence on the derived SO_2 dSCDs. The much stronger influence of the choice of the lower fit boundary is expected, because of several reasons:

- the SO_2 absorptions increase strongly towards short wavelengths
- the radiance decreases strongly towards short wavelengths
- the O_3 absorption strongly increases towards short wavelengths

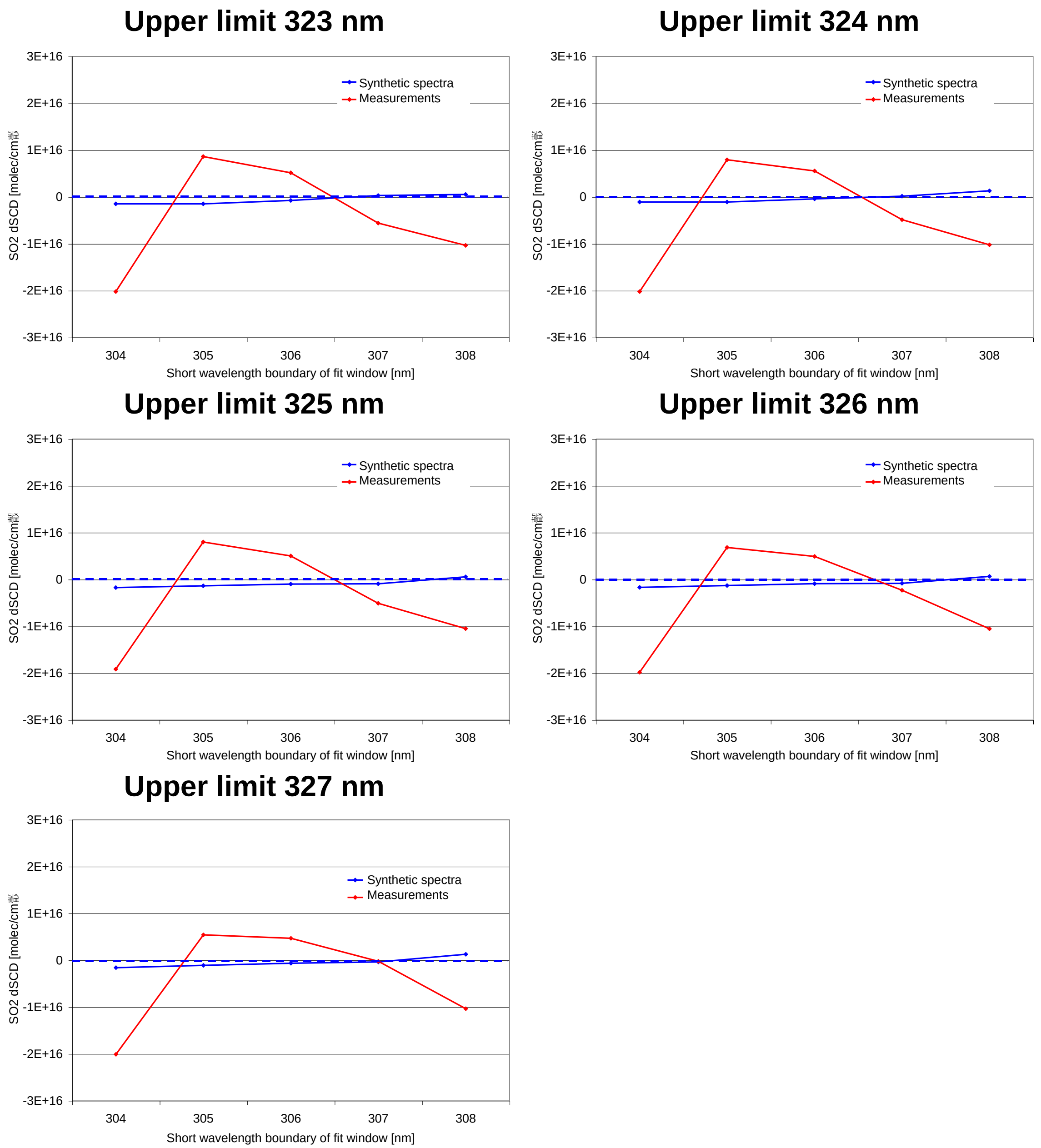

Fig. S11 Dependence of the fit results (for 1 °elevation) for the measured spectra (red lines) and synthetic spectra (blue lines) on the upper and lower boundaries of the fit range. Also shown are the ‘true dSCDs’ derived from the simulated air mass factors (blue dashed lines). The individual plots represent results for one fixed upper wavelength limit. The lower wavelength limit is represented by the x-axes.

Fit error and RMS

Figure S12 shows the SO_2 fit errors and RMS for synthetic (left) and measured spectra (right). Like for the analysis of BrO and HCHO, also for SO_2 systematically higher fit errors and RMS are found for the measured spectra. However, compared to BrO and HCHO, the difference is much larger for SO_2. This again indicates that the analysis of the measured spectra in the SO_2 analysis range is strongly affected by effects, which are not included in the simulation of the synthetic spectra (e.g. imperfect cross section, imperfect convolution). Thus for SO_2, only limited conclusions can be drawn from the synthetic spectra for the analysis of the real spectra. From the results of the measured spectra, the best lower limit of the fit range is probably found at about 305 – 306 nm (fit error) and 308 (RMS). For the upper limit of the fit range no clear dependence is found.

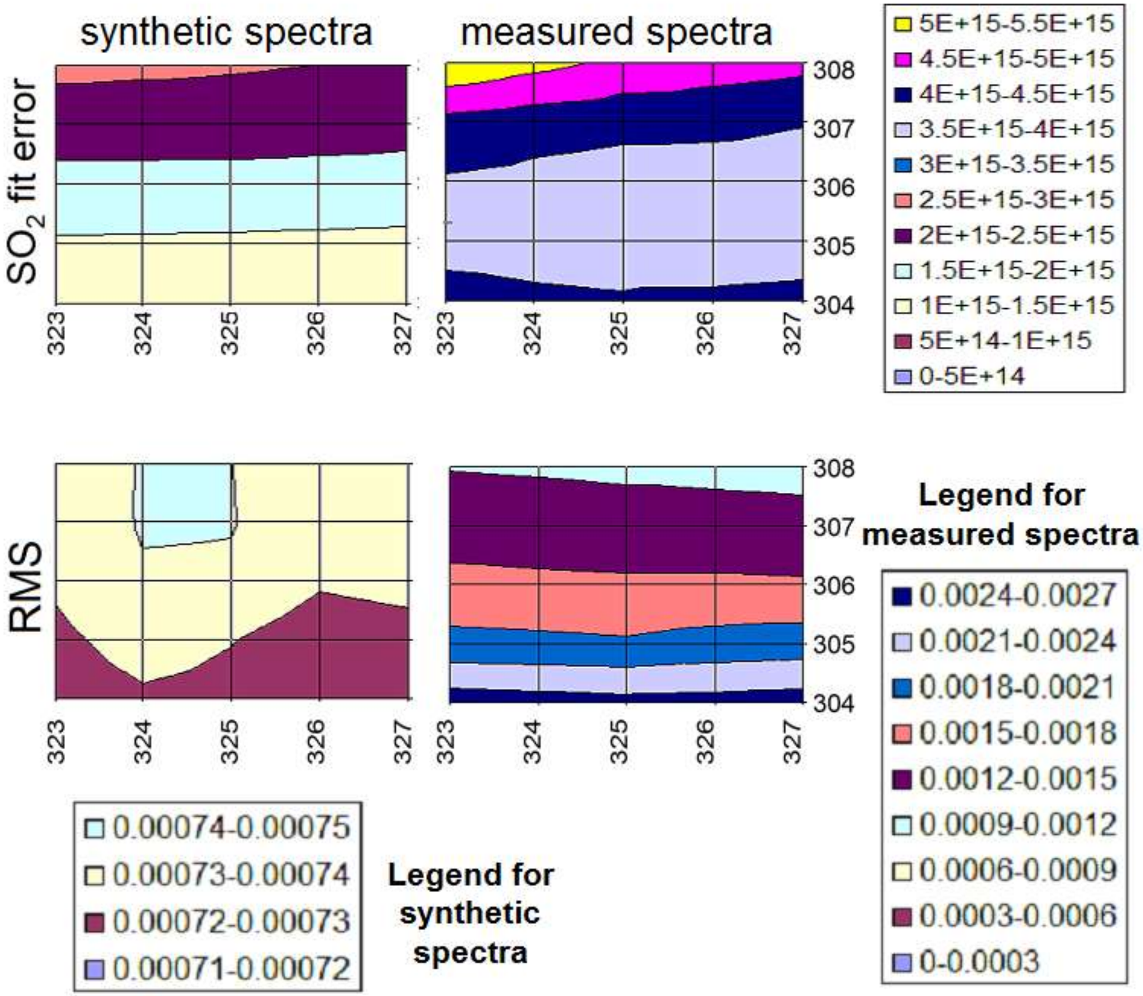

Fig. S12 Dependence of the SO_2 fit errors and RMS on the upper and lower boundaries of the fit range for the synthetic **(left)** and measured spectra **(right)**.

Standard deviation of the retrieved dSCDs and correlation between the dSCDs of SO_2 and O_3

In this section, the temporal variability of the derived SO_2 dSCDs and the correlation between the dSCDs of SO_2 and O_3 for 1° elevation are investigated. Although we don't make specific use of the O_3 retrieval results in this study, the correlation between the dSCDs of SO_2 and O_3 can be used to assess the quality of the SO_2 fit results. For the synthetic spectra the retrieved SO_2 dSCDs should be (close to) zero, because no SO_2 absorption was included in the simulation of the synthetic spectra. Also the O_3 absorption of all spectra should be the same. Accordingly, the correlation between the dSCDs of SO_2 and O_3 should also be (close to) zero. Some temporal variation is of course expected because of the added noise. For the measurements, the atmospheric trace gas concentrations can vary, and also changes of the atmospheric visibility might further contribute to a variation of the measured trace gas dSCDs. Thus the retrieved variability of the trace gas dSCDs for the measured spectra is expected to be higher than for the synthetic dSCDs. For the measured spectra, an (anti-) correlation of the derived dSCDs of SO_2 and O_3 might also reflect a (anti-) correlation of their true atmospheric absorptions. However, this is not very probably given the rather different profile shapes and formation processes. Thus a low correlation between the dSCDs of SO_2 is considered as an indication for a good fit quality also for the measured spectra.

Figure S13 shows the standard deviation of the time series of the SO_2 dSCDs for 1 ° elevation angle as well as the correlation coefficient between the dSCDs of SO_2 and O_3 for the synthetic (left) and measured spectra (right). As expected the standard deviations are higher for the measured spectra. Also the correlation between both species is higher for the measured spectra. Like for the fit error and the RMS, the differences between the results for the synthetic and measured spectra are much higher than for the BrO and HCHO analysis. This again indicates that for SO_2, only limited conclusions can be drawn from the synthetic spectra for the analysis of the real spectra. From the results of the measured spectra, the best lower limit of the fit range is found to be about 306 – 307 nm (SO_2 std) and 304 or 306 (correlation). For the upper limit of the fit range no clear dependence is found.

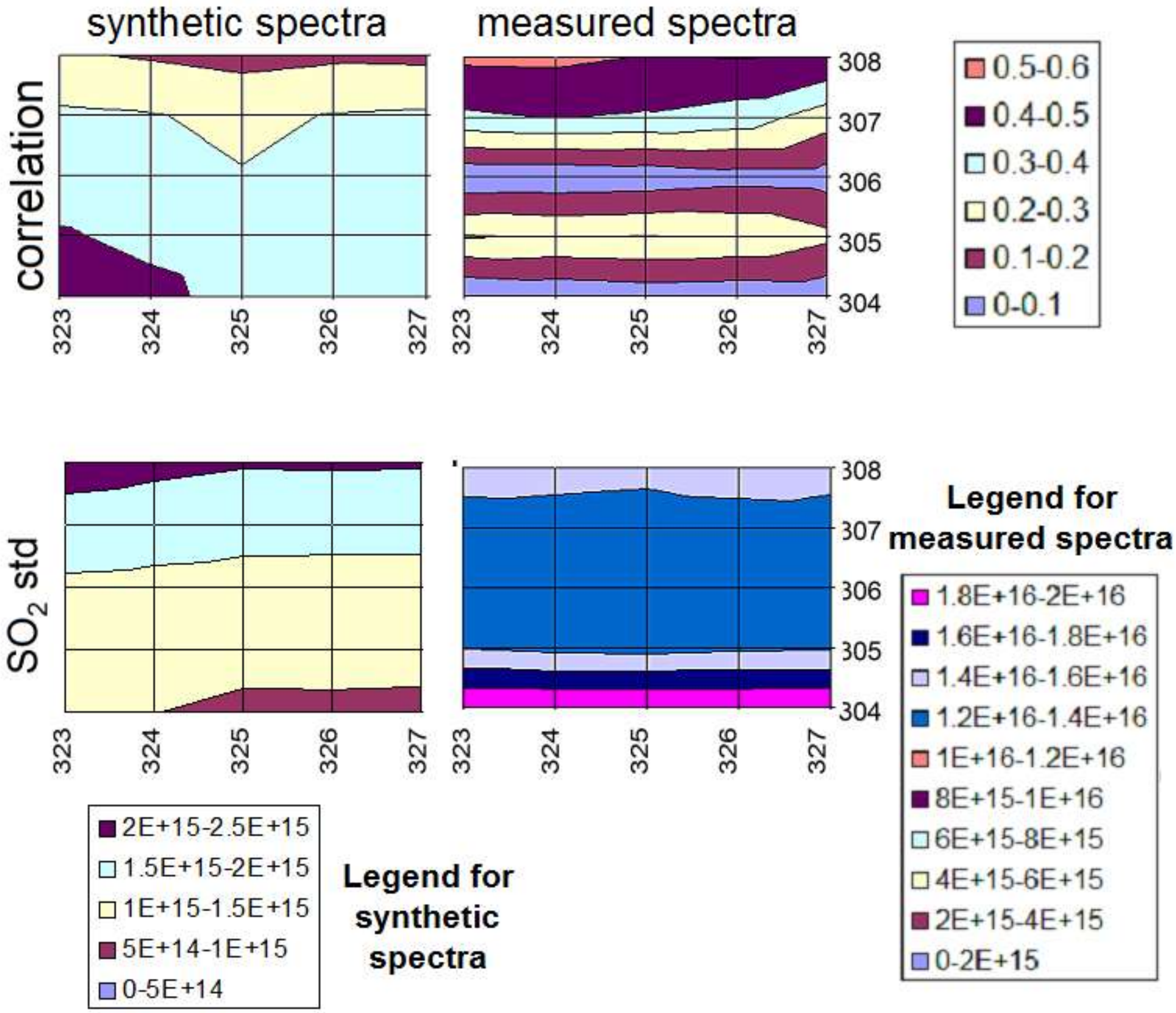

Fig. S13 Dependence of the variation (expressed as standard deviation) of the derived SO_2 dSCDs for 1 ° elevation angle and the correlation between the SO_2 and O_3 dSCDs (expressed as r^2) on the upper and lower boundaries of the fit range (**left:** synthetic spectra; **right:** measured spectra).

Final choice of fit the range

Based on the results from the previous sub section, the fit range from 306 to 325 nm is chosen for the analysis of SO_2. This choice is mainly based on the results for the measured spectra, because the synthetic spectra were found to be not representative for the real measurements (see discussion above). For the chosen fit range the lowest values of the fit error, the standard deviation of the SO_2 dSCD and the correlation between the dSCDs of SO_2 and O_3 were found.

Error estimate

The systematic and random uncertainties of the fit results for individual spectra (average of 10 original spectra) are summarized in Table S7.

Table S7 overview on the different systematic and random error sources

error source	**error of SO_2 fit result**
systematic errors	
Comparison of the fit results for the synthetic spectra to the ‘true dSCDs’	8e15 molec/cm²
random errors	
Fit error	4e15 molec/cm²
Standard deviation*	1.3e16 molec/cm²

*the standard deviation describes the total statistical error; at least part of the total statistical error is caused by the fit error.

The systematic error of the dSCDs is usually dominated by systematic effects of the spectral retrieval. These systematic effects are quantified by the comparison of the fit results for the measured and synthetic spectra. Only for high trace gas dSCDs the uncertainty of the cross section might become important. But for the rather low SO_2 dSCDs retrieved in this study the uncertainty of the cross section can be neglected.

For individual measurements, the random errors dominate the total uncertainty. However, if several measurements are averaged these errors can be largely reduced.

Quality filter

Spectra with bad fit quality have to be removed from further processing. First, measurements with a small number of individual scans (<800) are removed. This filter removes the worst fit results. In addition, a RMS filter is applied. Here a threshold for the RMS of 1.8e-3 is chosen. Figure S14 shows the frequency distribution of the RMS (for measurements with more than 800 scans). The RMS threshold removes about 24% of the SO_2 results.

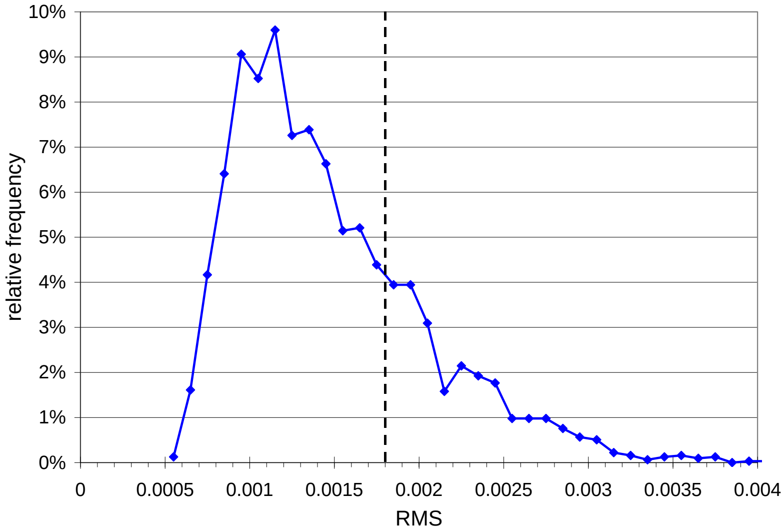

Fig. S14 Frequency distribution of the RMS of the spectral analysis of SO_2 for clear sky conditions. The vertical line indicates the threshold (0.0018) for removing measurements with high fit errors.

S3.3.3 Determination of the optimum fit range for NO_2

For the NO_2 analysis the exact determination of the fit range is less critical than for SO_2, HCHO, and BrO because of less atmospheric interfering. Moreover, the signal to noise ratio in the blue spectral range is larger than in the UV, and in particular it is more constant over the entire NO_2 fit range. Because of these reasons, less effort is spent on the determination of the NO_2 fit range, and in particular no synthetic spectra are used.

The spectral range of the instrument is 290 to 437 nm. Thus in principle a rather large spectral range from about 400 nm to 436 nm could be used. However, it turned out that large fit residuals occur for wavelength ranges with upper boundaries > 427nm (and also below 399nm, see Fig. S15). Thus for the NO_2 analysis a fit range between about 399 and 427 nm was chosen.

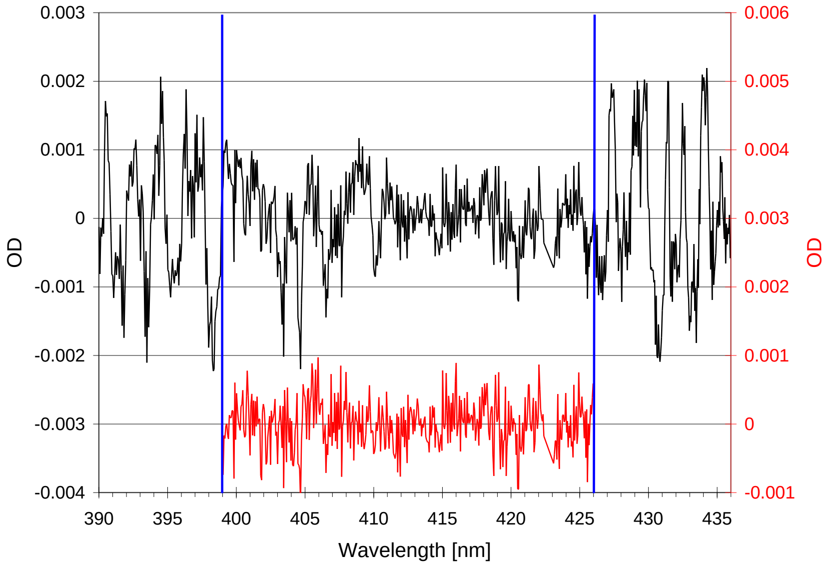

Fig. S15 Fit residuals for a NO_2 fit in two wavelength ranges (black: 390 – 436nm, left y-axis; red: 399 – 426 nm, right y-axis). The measurement (average of 10 individual measurements) was taken on 2 December 2012, 04:51 to 7:00. The (average) SZA and elevation angle were 59.3 ° and 6 °, respectively. The residual of the large spectral range shows strong systematic structures below 400nm and above 427 nm (RMS: 7.8e-4). The residual of the small spectral range shows much less systematic structures (RMS: 3.5e-4). The blue lines indicate the lower and upper boundaries of the finally chosen fit range 399 – 426nm.

To further specify the lower and upper fit boundaries, the RMS, fit errors, and the standard deviation for 1 ° elevation angle were derived for clear sky observations. The dependencies of these quantities on variations of the upper and lower fit boundaries are shown in Fig. S16. As expected, only weak dependencies were found. The final choice of the fit range was 399 – 426, because for that range the fit error and the standard deviation for measurements at 1 ° elevation were found to be smallest. However, the results for the other investigated fit ranges are very similar (the deviations are between -2e14 and +4e14 molec/cm^2), see Fig. S16.

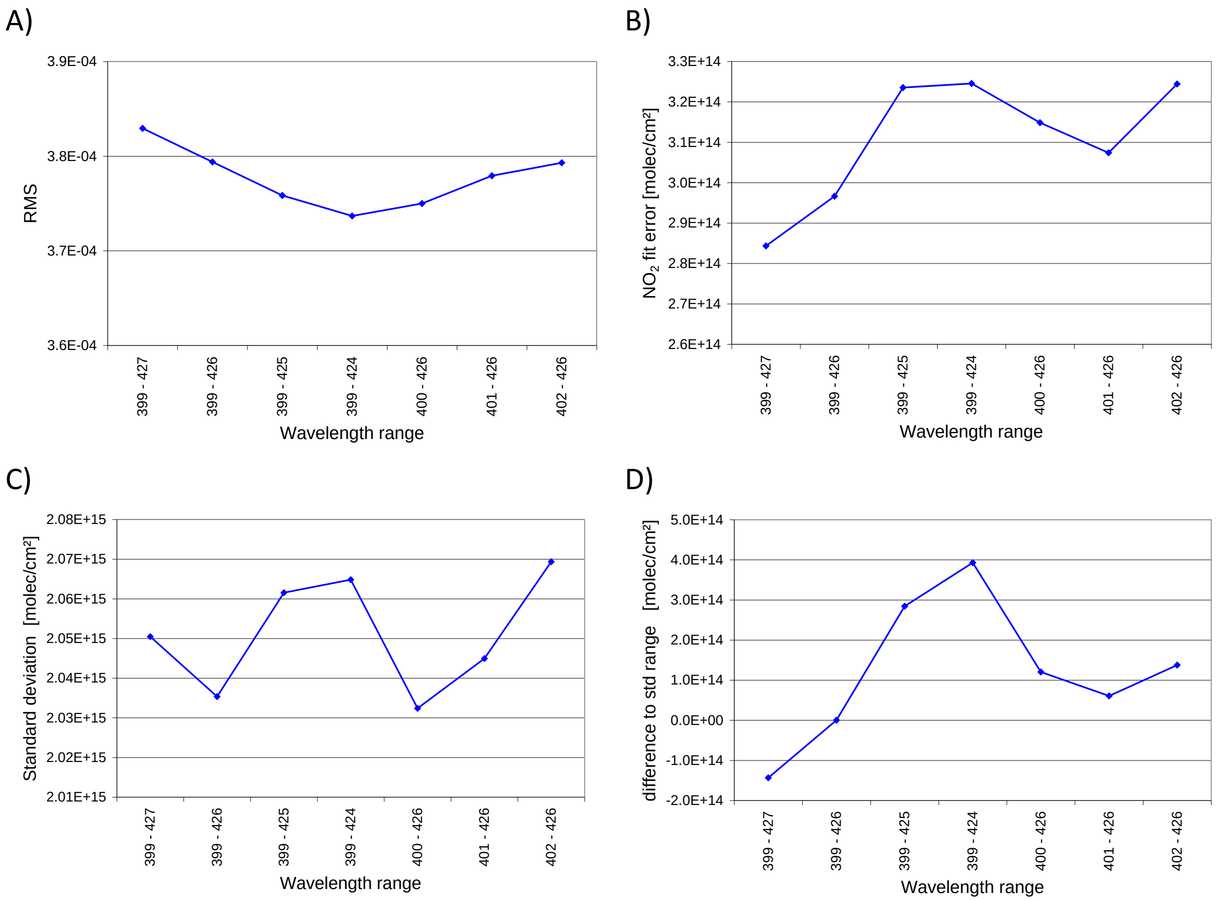

Fig. S16 Comparison of the fit results for different NO_2 fit ranges. **A)** Mean RMS; **B)** Mean NO_2 fit error; **C)** Standard deviation of NO_2 dSCDs for 1 °elevation angle; **D)** Mean difference of the NO_2 dSCDs with respect to the results for the fit range 399 – 426 nm.

Error estimate

The systematic and random uncertainties of the fit results for individual spectra (average of 10 original spectra) are summarized in Table S8.

The systematic error of the dSCDs is usually dominated by systematic effects of the spectral retrieval. These systematic effects are quantified by the comparison of the fit results for the different spectral ranges. Only for high trace gas dSCDs the uncertainty of the cross section might become important. But for the rather low NO_2 dSCDs retrieved in this study the uncertainty of the cross section can be neglected.

For individual measurements, the random errors dominate the total uncertainty. However, if several measurements are averaged these errors can be largely reduced.

Table S8 overview on the different systematic and random error sources

error source	**error of NO_2 fit result**
systematic errors	
Deviation of NO_2 dSCDs for different fit ranges	6e14 molec/cm²
random errors	
Fit error	3e14 molec/cm²
Standard deviation*	2e15 molec/cm²

*the standard deviation describes the total statistical error; at least part of the total statistical error is caused by the fit error.

Quality filter

Spectra with bad fit quality have to be removed from further processing. First, measurements with a small number of individual scans (<800) are removed. This filter removes the worst fit results. In addition, a RMS filter is applied. Here a threshold for the RMS of 5e-4 is chosen. Figure S17 shows the frequency distribution of the RMS (for measurements with more than 800 scans). The RMS threshold removes about 10% of the NO_2 results.

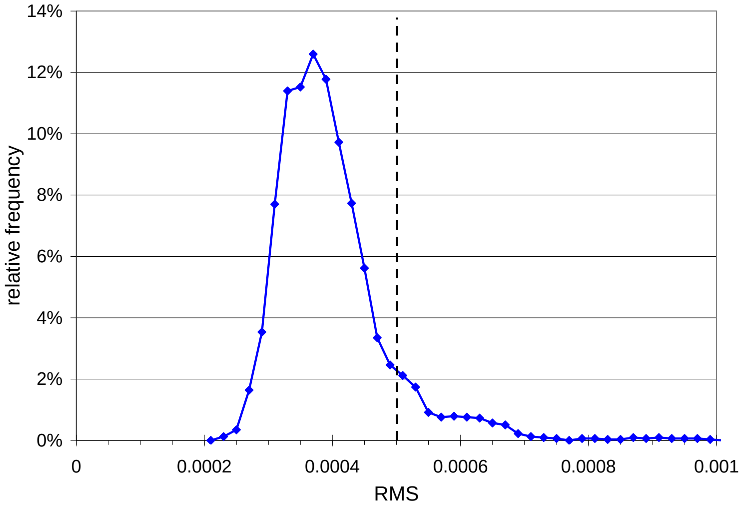

Fig. S17 Frequency distribution of the RMS of the spectral analysis of NO_2 for clear sky conditions. The vertical line indicates the threshold (0.0005) for removing measurements with high fit errors.

S4 Input trace gas profiles for the radiative transfer simulations

S4.1. NO_2, SO_2 and HCHO

The SO_2 vertical concentration profile is determined assuming a constant mixing ratio throughout the atmosphere. Of course this is a rather strong simplification of the true profiles, which usually have much more complex shapes. But from the measurements, no information about the true atmospheric SO_2 profile can be derived, because the measured SO_2 dSCDs are below the detection limit. Nevertheless, based on this simple assumption it is still possible to estimate the approximate upper limit or the tropospheric SO_2 mixing ratio from the measured SO_2 dSCDs. For NO_2 and HCHO we assumed two profile shapes: first, like for SO_2 a constant mixing ratio throughout the troposphere was assumed. Second, modified profile shapes were chosen (red lines in Fig. S18), which fit best to the measured elevation angle dependence of both trace gases (see Fig. S20). For both trace gases it became obvious that the measured elevation angle sequence can only be (approximately) matched if enhanced trace gas concentrations are present in the layer close to the instrument (between 3700m and 4300m). For HCHO the best match with the measured elevation dependence is even found if enhanced HCHO mixing ratios are only present in these layers. Fortunately, for the estimation of the NO_2 and HCHO mixing ratios, the exact profile assumptions are not critical. The relationships between the measured trace gas dSCDs at 1 ° elevation and the corresponding mixing ratios in the atmospheric layer close to the instrument are very similar:

NO_2: a dSCD of 1×10^{15} molec/cm^2 corresponds to a mixing ratio of 23 ppt (constant mixing ratio) or 33 ppt (modified profile)

HCHO: a dSCD of 1×10^{15} molec/cm^2 corresponds to a mixing ratio of 42 ppt ppt (constant mixing ratio) or 55 ppt (modified profile)

In Fig. S18 the trace gas concentration profiles used in the RTM simulations are shown. They are calculated for typical background mixing ratios of the trace gases. However, it should be noted that the exact knowledge of the true mixing ratio is not important, because for these weak atmospheric absorbers, the air mass factors are almost independent from the absolute trace gas concentrations.

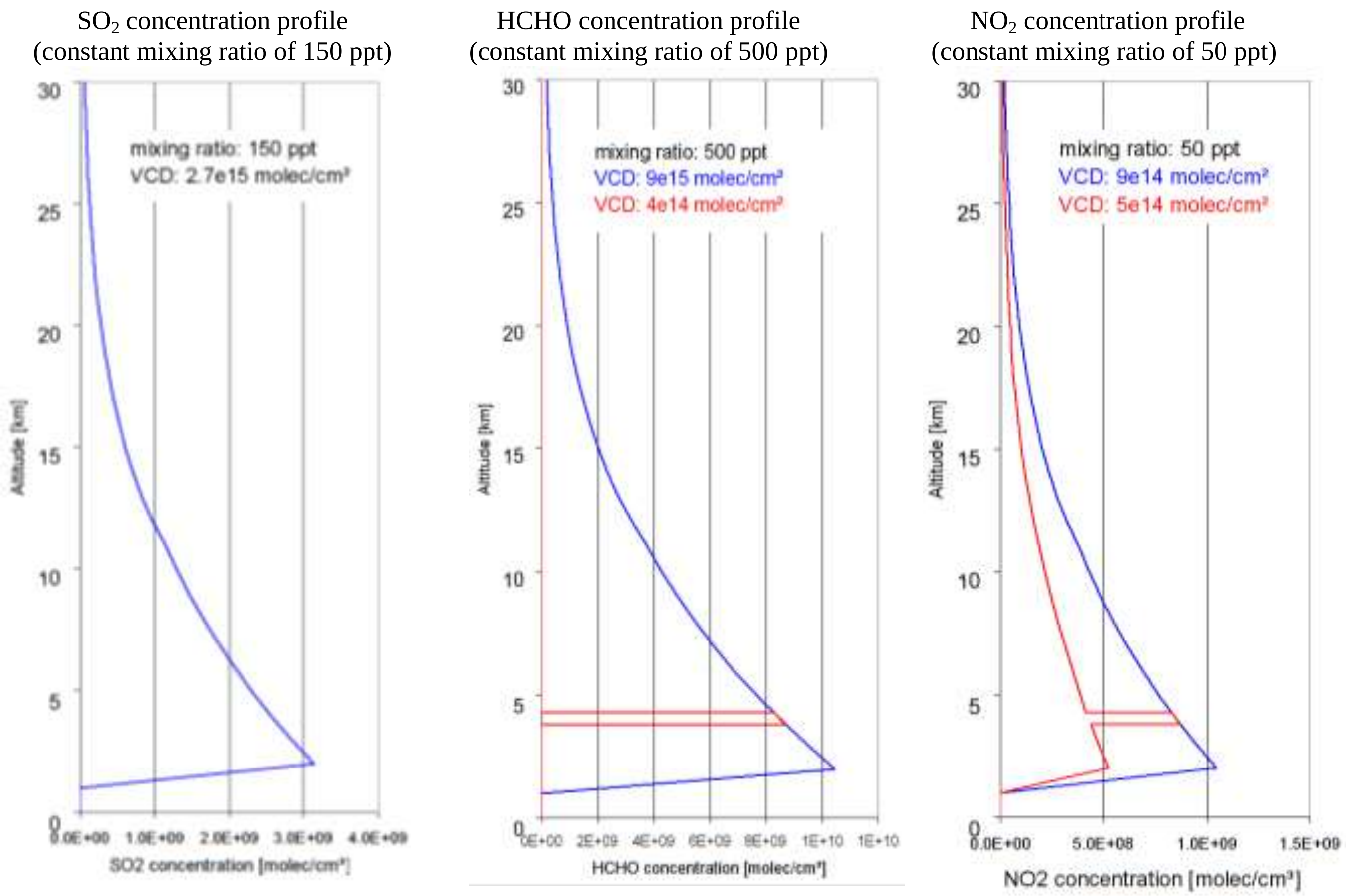

Fig. S18 Vertical concentration profiles of SO_2, HCHO, and NO_2 used in the radiative transfer simulations. For HCHO and NO_2 two profiles were used: One profile (blue) assumes a constant mixing ratio in the troposphere, the other (red) shows profiles which fit best to the measured elevation angle dependence (see Fig. S20). In the figures also the corresponding vertical column densities (VCDs) are given.

In Fig. S19 the trace gas dSCDs of NO_2, SO_2, and HCHO corresponding to the input profiles with constant mixing ratios in the troposphere are shown as a function of the elevation angle. The trace gas dSCDs are given for different aerosol loads and for different seasons (left: summer; right: winter). Interestingly, for HCHO and SO_2, the dSCDs at 1 ° elevation angle are almost independent from the aerosols load. In contrast, for the NO_2 dSCDs at 1 °elevation angle a larger dependence on the aerosol load is found, probably because of less Rayleigh scattering at these longer wavelengths. Nevertheless, for simulations with AODs between 0.1 and 0.5, also the NO_2 dSCDs at 1 °elevation angle very similar.

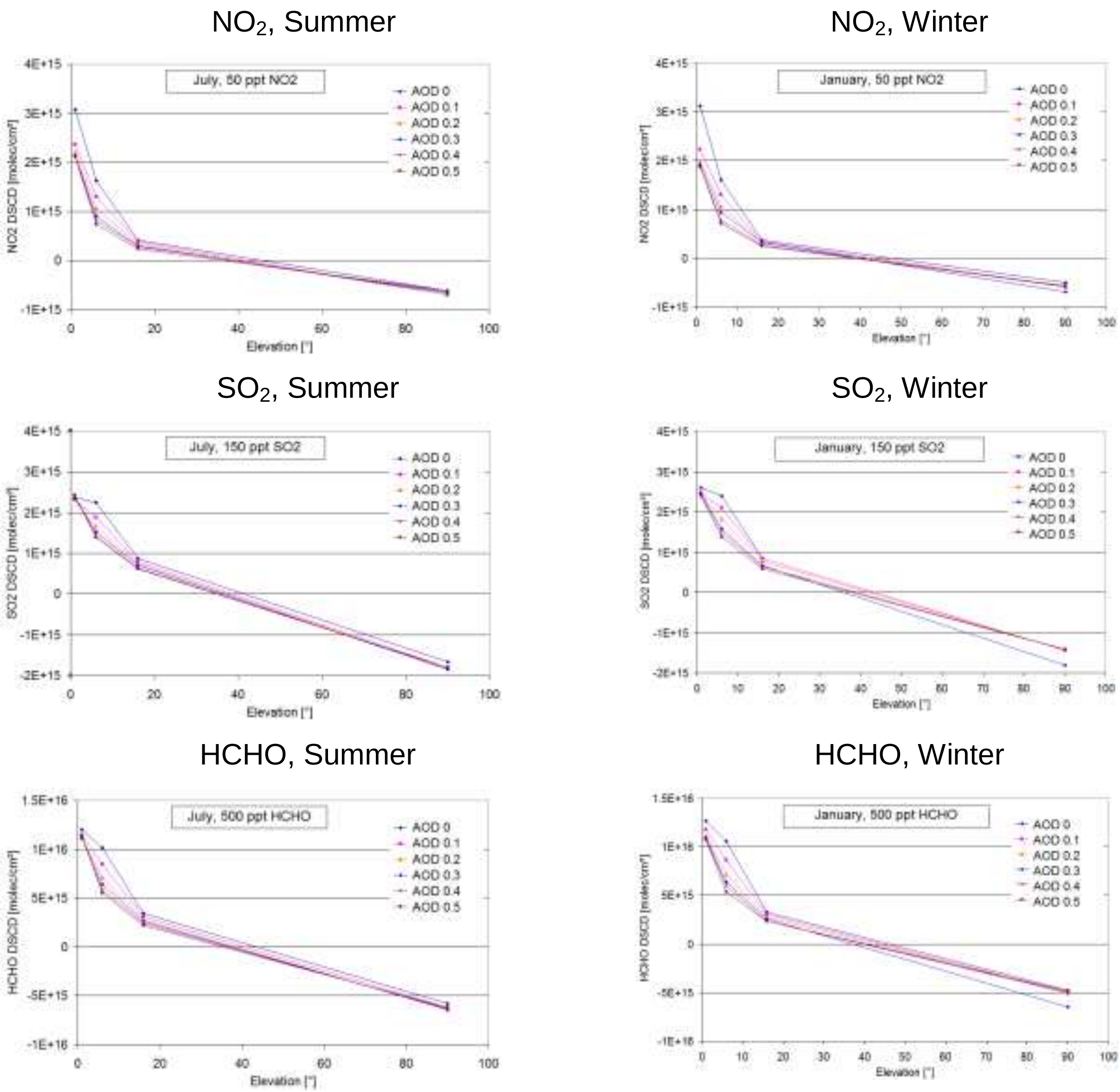

NO$_2$, Summer

NO$_2$, Winter

SO$_2$, Summer

SO$_2$, Winter

HCHO, Summer

HCHO, Winter

Fig. S19 Trace gas dSCDs simulated for the profiles with constant mixing ratios shown in Fig. 6 for summer **(left)** and winter **(right)**. The individual lines represent results for different aerosol loads.

Figure S20 compares the average elevation angle dependence of the measured NO$_2$ and HCHO dSCDs (see also Fig. 8) with simulated dAMFs for different profile assumptions. From this comparison it becomes obvious that the simulations for constant mixing ratios do not fit the measured elevation dependences. The discrepancies are especially large for HCHO indicating that most of the HCHO resides in atmospheric layers close to the instrument. Here it should be noted that no perfect agreement should be expected, because of the rather simplistic comparison (using averaged results from all seasons). Nevertheless, as mentioned above, the conversion of the measured NO_2 and HCHO dSCDs into trace gas mixing ratios in the atmospheric layers close to the instrument is only weakly affected by the profile assumptions.

We also investigated the effect of the uncertainty of the elevation calibration (±0.5°) on the simulated dAMFs by performing simulations with modified elevation angles. Changes of the elevation angle by ±0.5° have a very small effect on the dAMFs for high elevation angels (<2%) and are therefore negligible. For 1° elevation angle the effects can become larger and are given below for the different trace gases and profile assumptions:

SO_2, constant mixing ratio:	<5%
NO_2, constant mixing ratio:	<5%
NO_2, modified profile:	<20%
HCHO, constant mixing ratio:	<5%
HCHO, modified profile:	<15%
BrO	<1%

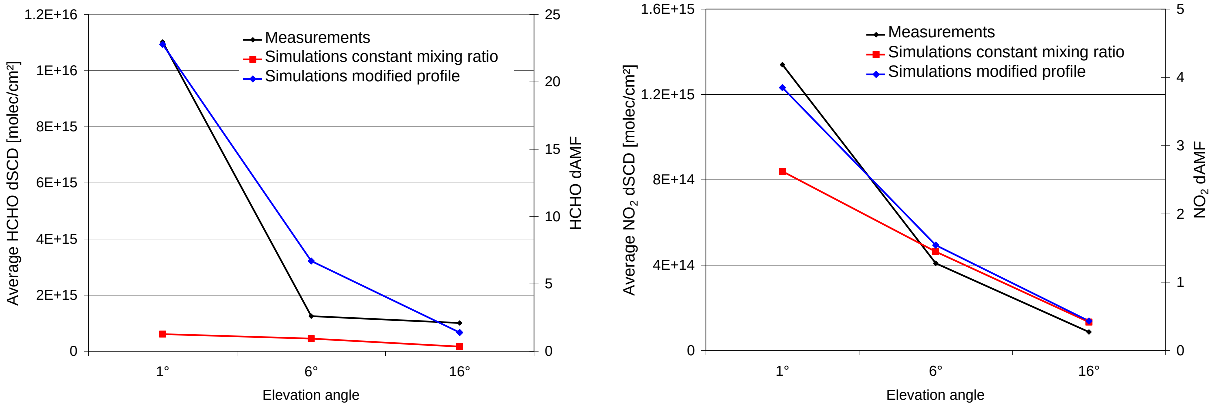

Fig. 20 Average elevation angle dependence of HCHO (left) and NO_2 (right) for measurements at clear sky and low aerosol load. Black lines: measured average dSCDs (left axes); red: simulated dAMFs assuming constant mixing ratios in the troposphere; blue: simulated dAMFs for modified trace gas profiles (see Fig. S18).

S4.2 BrO

For BrO the effect of the stratospheric BrO cannot be separated from the effect of (possible) tropospheric BrO absorptions. This is caused by the fact that the maximum of the stratospheric BrO is usually found only a few kilometres above the tropopause. Thus, the BrO dSCDs retrieved for the stratospheric BrO absorption depend systematically on the elevation angle. Moreover, variations of the tropopause height directly influence the stratospheric BrO profile. Thus the measured BrO dSCDs become systematically dependent also on the tropopause height. Dort et al. (2008) investigated the dependence of the stratospheric BrO mixing ratios as a function of the relative altitude with respect to the tropopause height (see Supplement Sect. 5.2 and Fig. S24). The mixing ratio profile presented in Dorf et al. (2008) was also used in this study to calculate BrO concentration profiles as a function of the tropopause height (see Fig. S21).

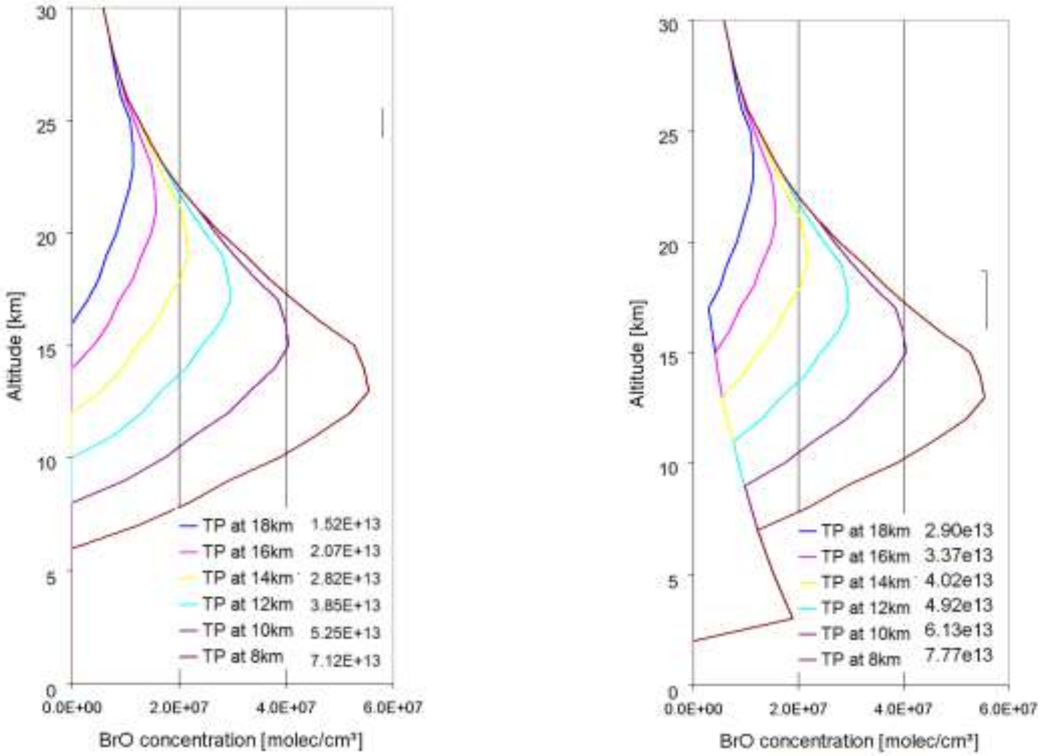

Fig. S21 BrO concentration profiles as function of the tropopause height. **Left:** no BrO in the troposphere; **right:** 1ppt BrO in the troposphere (above 3km). The numbers in the figures represent the corresponding BrO VCDs.

S5 Influence of stratospheric trace gas abundances on the MAX-DOAS results

S5.1 NO_2

In this section the influence of the stratospheric NO_2 absorption on the MAX-DOAS measurements at the WLG station are investigated. The underlying question is whether the simulation of the stratospheric and tropospheric absorptions can be separated (which makes the direct interpretation of the MAX-DOAS results much easier). To answer that question, the NO_2 dSCDs observed by the MAX-DOAS measurements corresponding to the stratospheric NO_2 absorption are simulated. For the radiative transfer simulations stratospheric NO_2 profiles provided by the study from Bauer et al. (2012) were used. They provide profiles for different seasons and latitude bands. Since the WLG station is located close to the border between two latitude bands (30 °S to 30 °N, and 30 ° to 60 °N), the average of the profiles of both latitude bands were used. Two stratospheric profiles were derived, one for summer and one for winter (see Fig. S22).

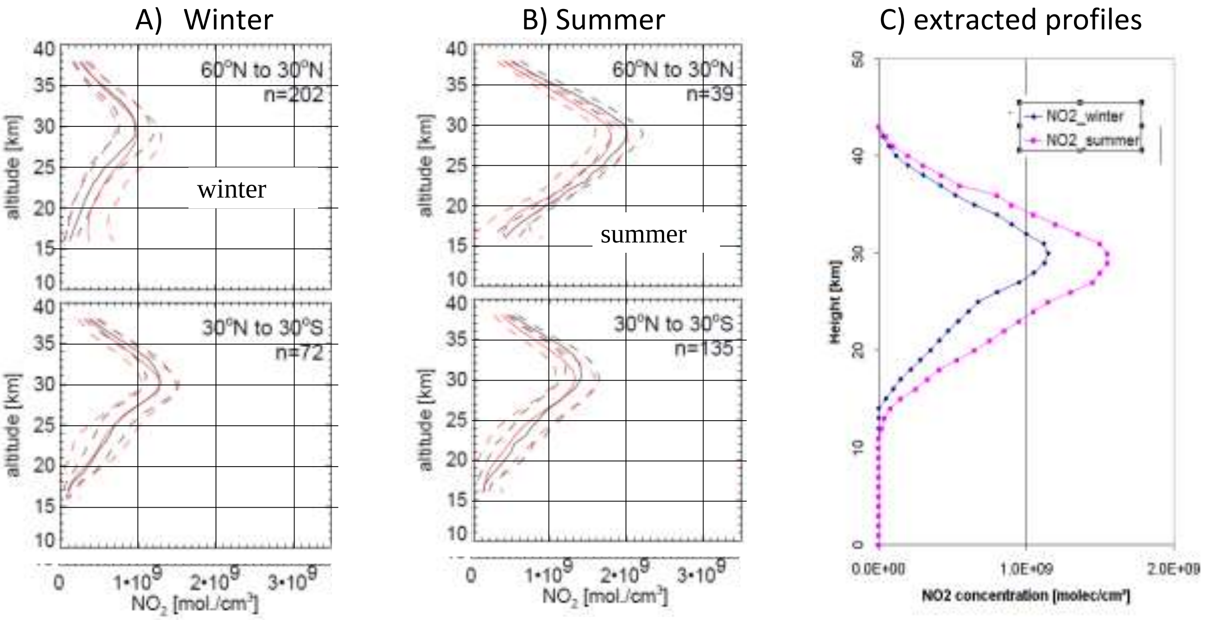

Fig. S22 Stratospheric profiles taken from the study of Bauer et al. (2012) for Winter **(A)** and Summer **(B)** for the tropics and northern mid-latitudes. The right figure **(C)** shows the extracted profiles for summer and winter, which were used for the radiative transfer simulations. The corresponding VCDs are: 1.51e15 molec/cm^2 (winter) and 2.30e15 molec/cm^2 (summer).

In Fig. S23 the corresponding dSCDs simulated for the MAX-DOAS measurements at different elevation angles are shown. The deviations of the NO_2 dSCDs from zero are largest for 1 ° elevation angles. They are about -1e14 molec/cm^2 in winter and between -2e14 molec/cm^2 and -1e14 molec/cm^2 in summer. Thus they are about one order of magnitude smaller than the observed NO_2 dSCDs (see Sect. 6.1). For the quantitative interpretation of the measured NO_2 dSCDs they can therefore be neglected.

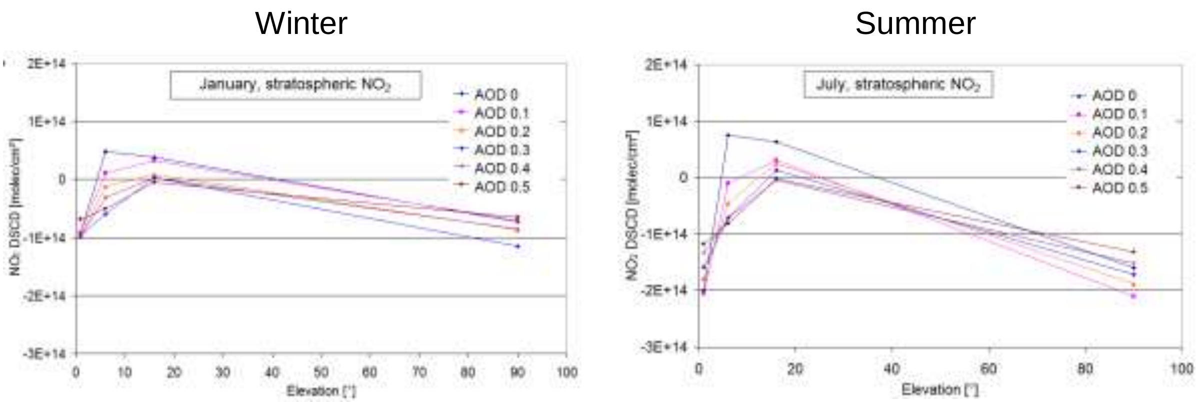

Fig. S23 Simulated NO_2 dSCDs for the stratospheric profiles shown in Fig. **S22 (right)** for winter **(left)** and summer (right).

S5.2 BrO

The stratospheric BrO profiles were constructed following the study of Dorf et al. (2008) who described the stratospheric BrO mixing ratio relative to the altitude of the tropopause height (Fig. S24A). We used their parameterisation, but with a slightly lower maximum BrO mixing ratio of 15 ppt instead of 16 ppt in order to account for the decrease of the stratospheric BrO load between the study of Dorf et al. (2008) and the measurements considered in this study. The two sub figures at the right side of Fig. S24 show the derived BrO height profiles for different tropopause layer heights. In Fig. S24B it is assumed that no BrO exists in the troposphere; in Fig. S24C a background BrO mixing of 1 ppt was assumed. The corresponding BrO dSCds are shown in Figs. S25 and S26. Interestingly, negative BrO dSCDs are found for measurements at 1 °elevation angle if no BrO was assumed in the troposphere (Fig. S25). Substantially higher BrO dSCDs are found for the cases when a tropospheric background concentration of 1 ppt was assumed (Fig. S26).

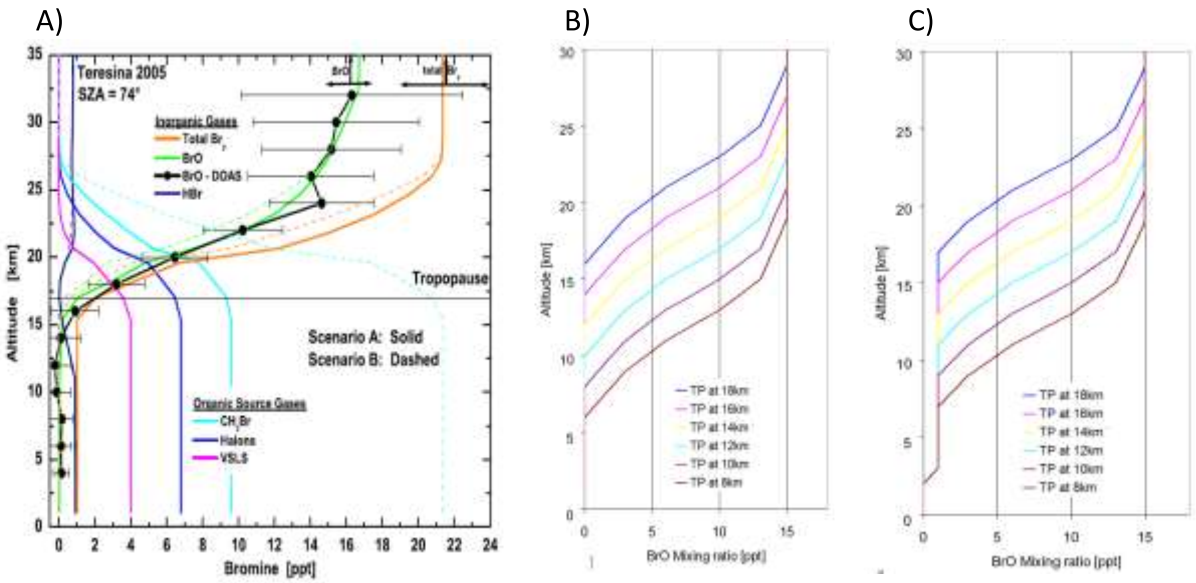

Fig. S24 in Fig **A):** as Fig. 1 in Dorf et al. (2008): The green line represents the BrO mixing ratios derived from various measurements and model simulations as function of the relative height with respect to the tropopause (horizontal black line). In the two figures at the right the corresponding BrO mixing ratios are plotted as function of different tropopause heights. In Fig. **B)** no BrO was assumed in the troposphere; in Fig. **C)** a constant BrO mixing ratio of 1 ppt was assumed in the troposphere. Note that the decrease of the stratospheric BrO mixing ratio between 2008 and the period of the Tibet measurements of about -1 ppt was taken into account.

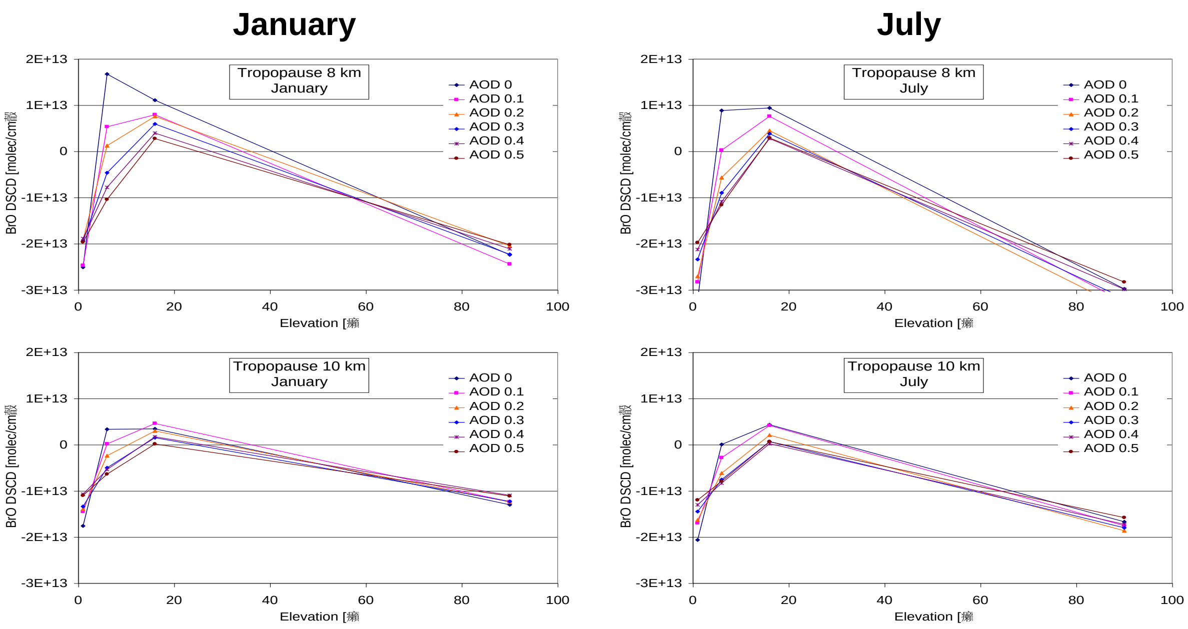

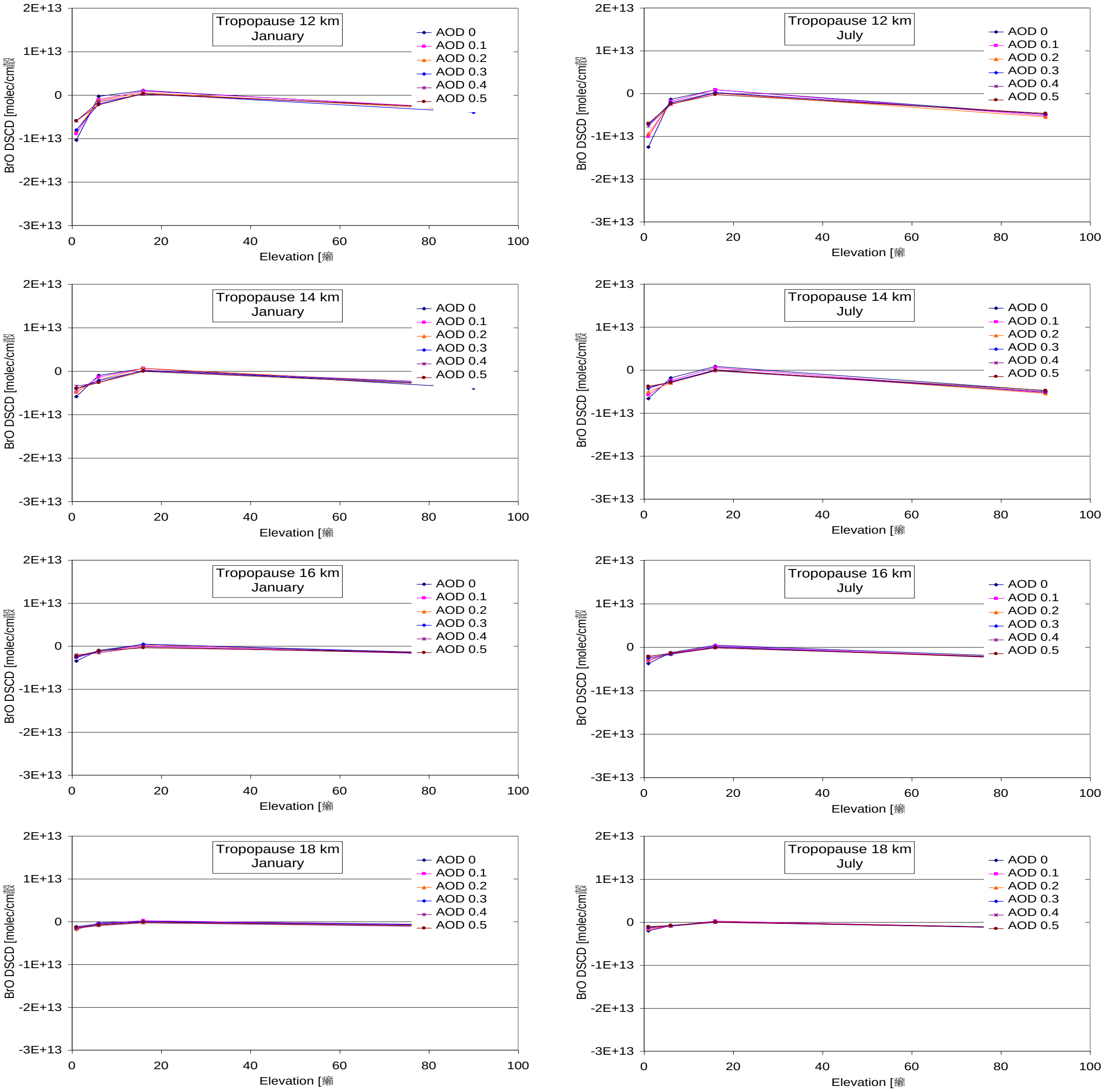

Fig. S25 BrO dSCDs calculated for the profiles shown in Fig. **S24**B with zero BrO concentrations in the troposphere for different tropopause heights (**left:** winter; **right:** summer).

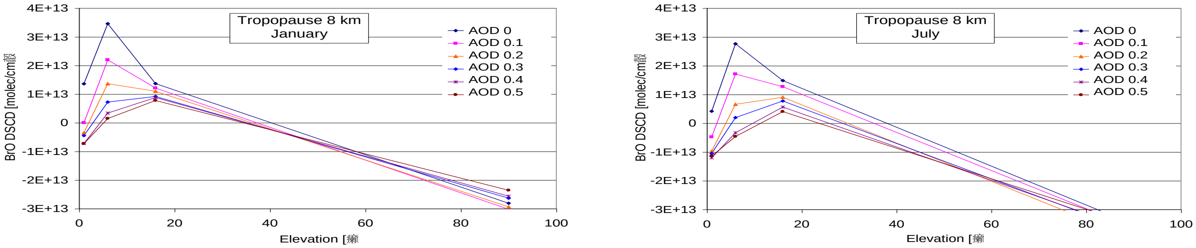

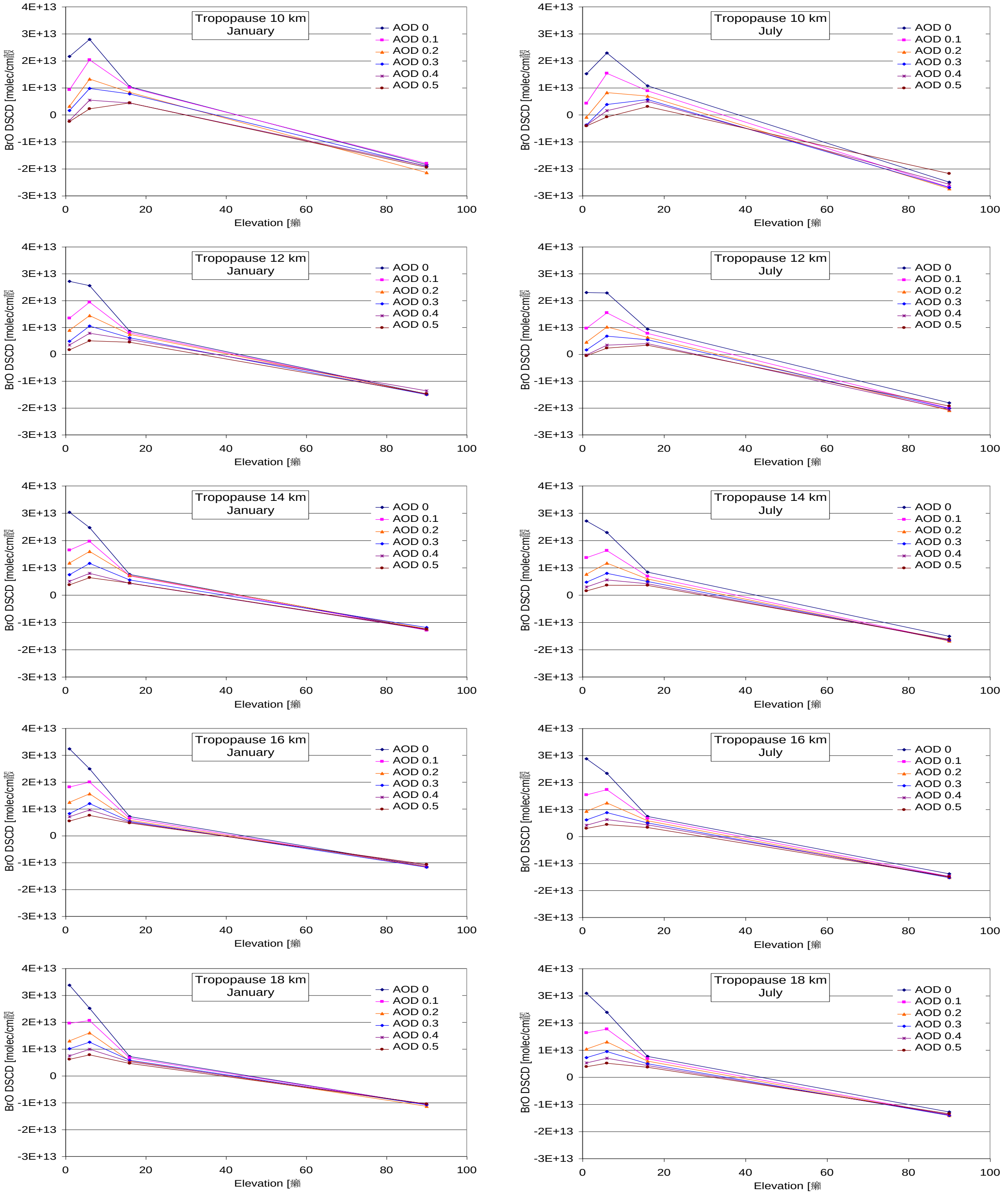

Fig. S26 BrO dSCDs calculated for the profiles shown in Fig. **S24**C with 1 ppt BrO in the troposphere for different tropopause heights (**left:** winter; **right:** summer).

S6 Cloud and aerosol filters

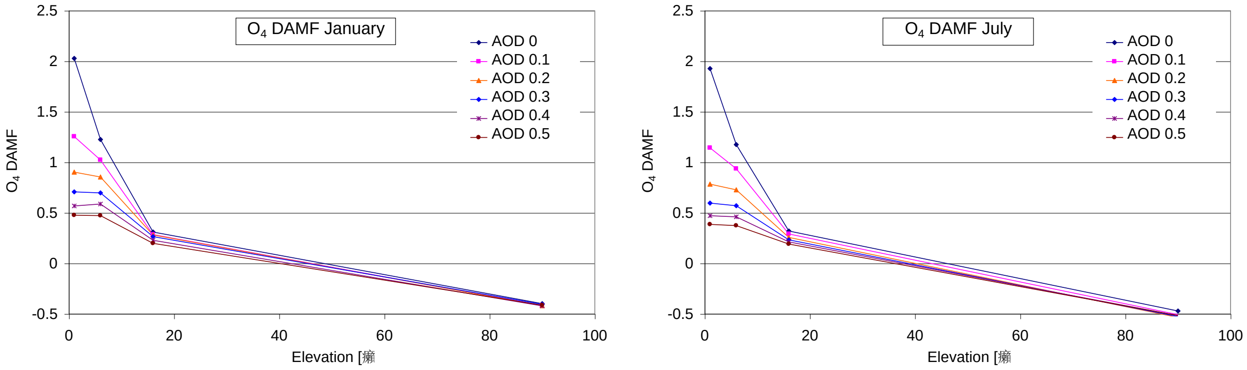

Fig. S27 Simulated O$_4$ dAMFs for different aerosol loads for winter **(left)** and summer **(right)**. Constant aerosol extinction was assumed between 2600 and 5600m.

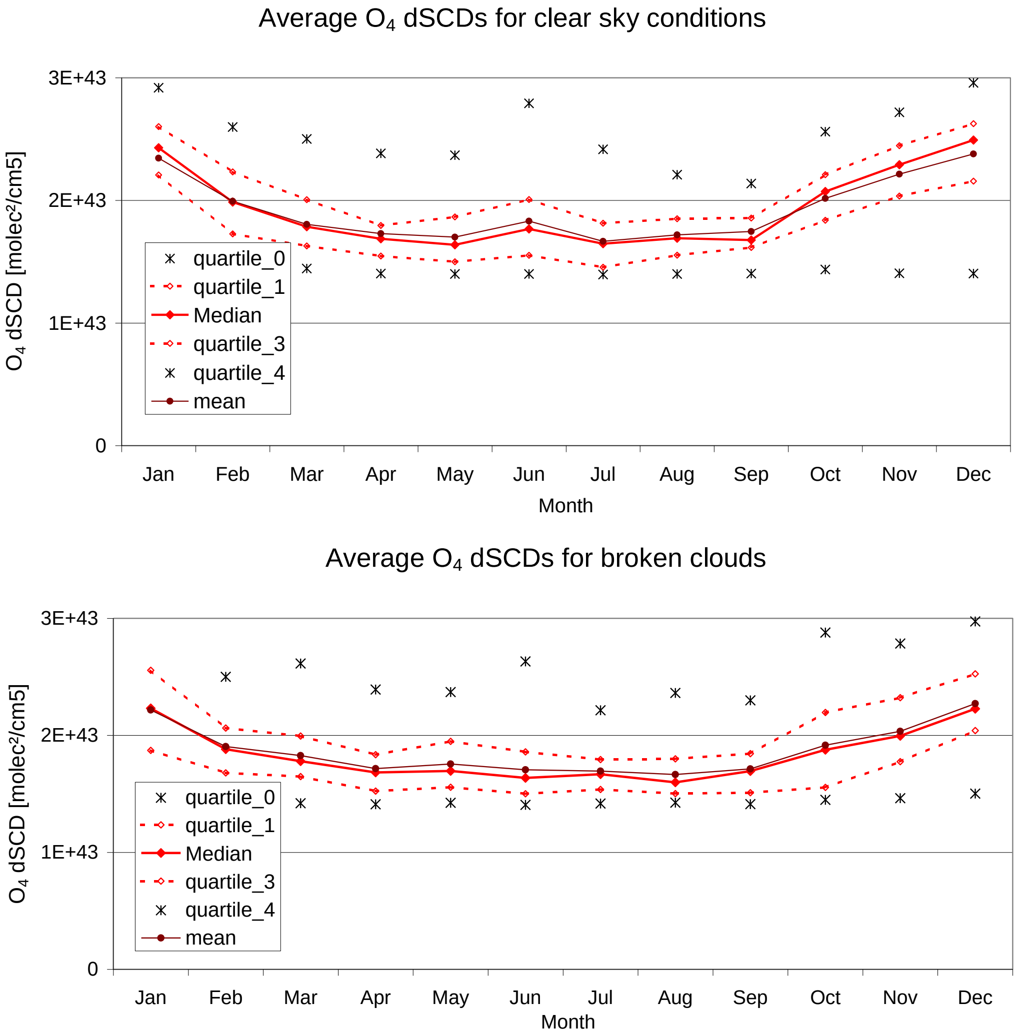

Fig. S28 O_4 dSCDs at 1 ° elevation for clear sky **(top)** and broken clouds **(bottom)** spectra (averages of 10 original spectra for 2012 - 2015) with number of scans > 800 and RMS of the O_4 fit < 2e-3.

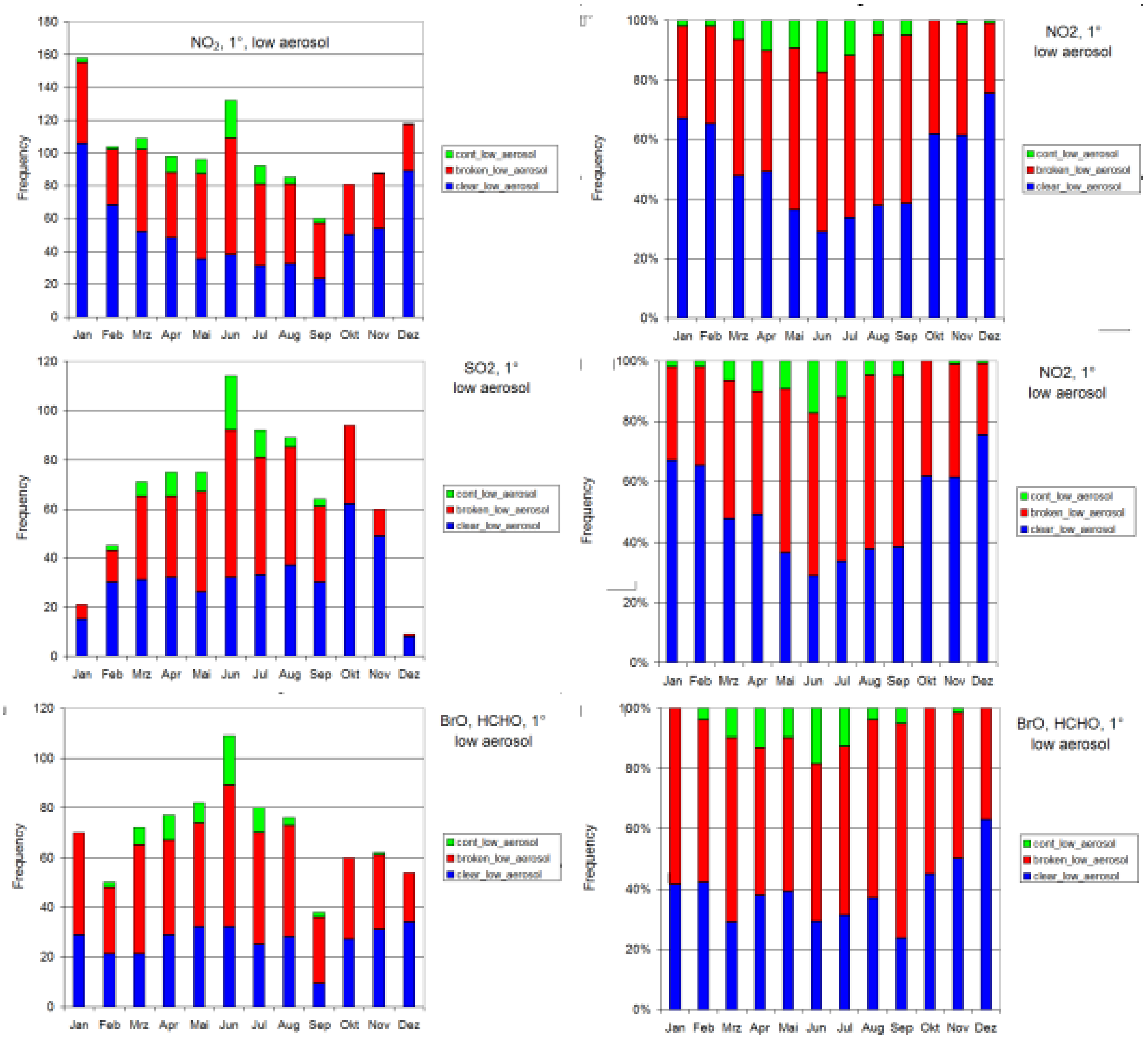

Fig. S29 Absolute **(left)** and relative **(right)** frequency of the different sky conditions for results of selected trace gases (top: NO$_2$, middle: BrO and HCHO, bottom: SO$_2$). The statistics are based on the number of observations at 1 ° elevation angle (mean of 10 original spectra from April 2012 to April 2015). In addition to the filter for the removal of high aerosol loads, also the specific RMS filters for the different trace gases are applied (see Supplement Sect. 3.3).

S7 Seasonal means of the dSCDs under broken cloud conditions

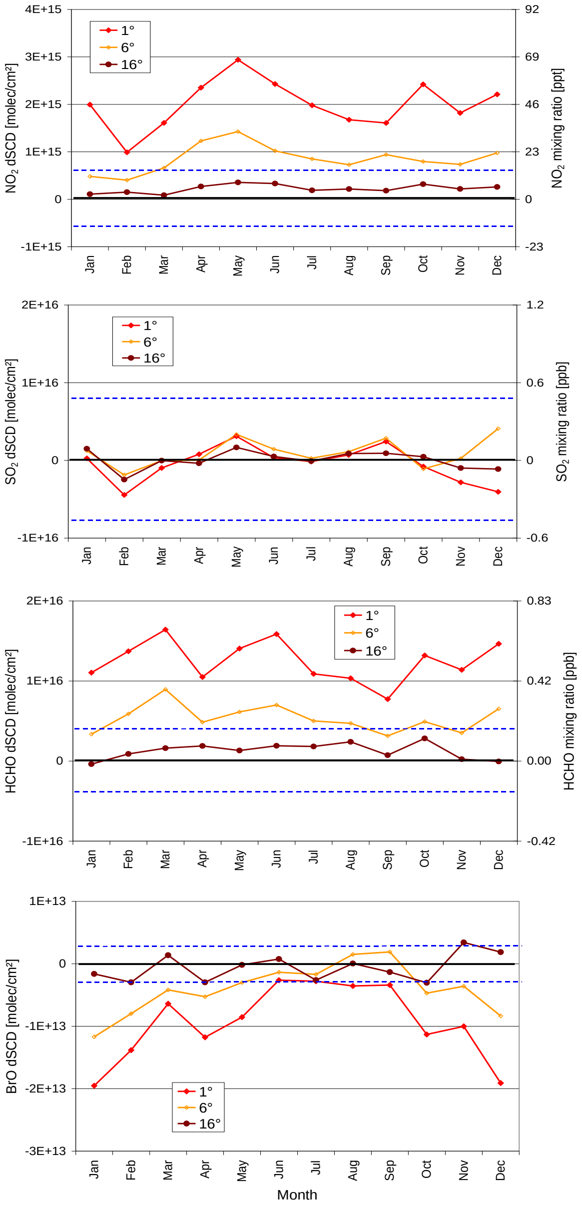

Figure S30 Seasonal means of the trace gas dSCDs for different elevation angles for broken clouds and low aerosol load. For NO_2, SO_2, and HCHO the right axes represent the approximate mixing ratios for measurements at 1 ° elevation angle. The blue dotted lines indicate the systematic uncertainties, which can be considered as lower bound of the detection limit.

S8 Estimation of tropospheric BrO mixing ratios from the measured BrO dSCDs

Fig. S31 shows the dependence of the measured BrO dSCDs for different elevation angles together with simulation results for tropospheric background mixing ratios of 0 ppt or 1 ppt. While for 1 ° elevation a strong dependence on the tropopause height is found, such a dependency is not observed for the higher elevation angles. These findings are consistently found for the measurements and simulations (but the measured BrO dSCDs show a rather large scatter). Interestingly, the differences between the simulated BrO dSCDs for 0 and 1 ppt tropospheric background are almost constant. This finding indicates that the increase of the measured BrO dSCDs (with respect to a simulation without a tropospheric BrO background) caused by an increase of the tropospheric BrO background is almost proportional to the tropospheric BrO mixing ratio.

For the estimation of the (upper limit of the) tropospheric BrO background the measurements at 1 ° elevation angle are chosen, because they are most sensitive to BrO absorptions in the troposphere (the difference between the simulations for 0 and 1 ppt in Fig. S31 are largest for an elevation angle of 1 °). To account for the dependence on the tropopause height the following procedure was applied:

First the measured BrO dSCDs are subtracted from the simulated BrO dSCDs for the same tropopause height. This is done for the simulations for 0 ppt as well as 1 ppt background BrO. From the obtained differences the man values and the standard deviations are calculated. For 0 ppt the mean difference is $0.9*10^{13}$ molec/cm^2, for 1 ppt it is $2.4*10^{13}$ molec/cm^2. The standard deviation for both differences is $1.0*10^{13}$ molec/cm^2.

In the next step the total error (of the difference between simulations and measurements) is calculated as the sum of the standard deviation and the estimate for the systematic error of $0.3*10^{13}$ molec/cm^2 (see Supplement Sect. 3.3.3).

In the final step the total error ($1.3*10^{13}$ molec/cm^2) is compared to the mean values of the differences for 0 ppt and 1 ppt. The total error is found above the mean difference for the simulations for 0 ppt BrO ($0.9*10^{13}$ molec/cm^2), and below the mean difference for the simulations for 1 ppt BrO ($2.4*10^{13}$ molec/cm^2). Assuming that the (increase of the) measured BrO dSCD depends linearly on the BrO background mixing ratio (see above), an upper limit for the BrO background mixing ratio of 0.23 ppt is obtained. From similar calculations for 6 ° and 16 ° elevation, upper limits of 0.34 ppt and 0.60 ppt are found, respectively.

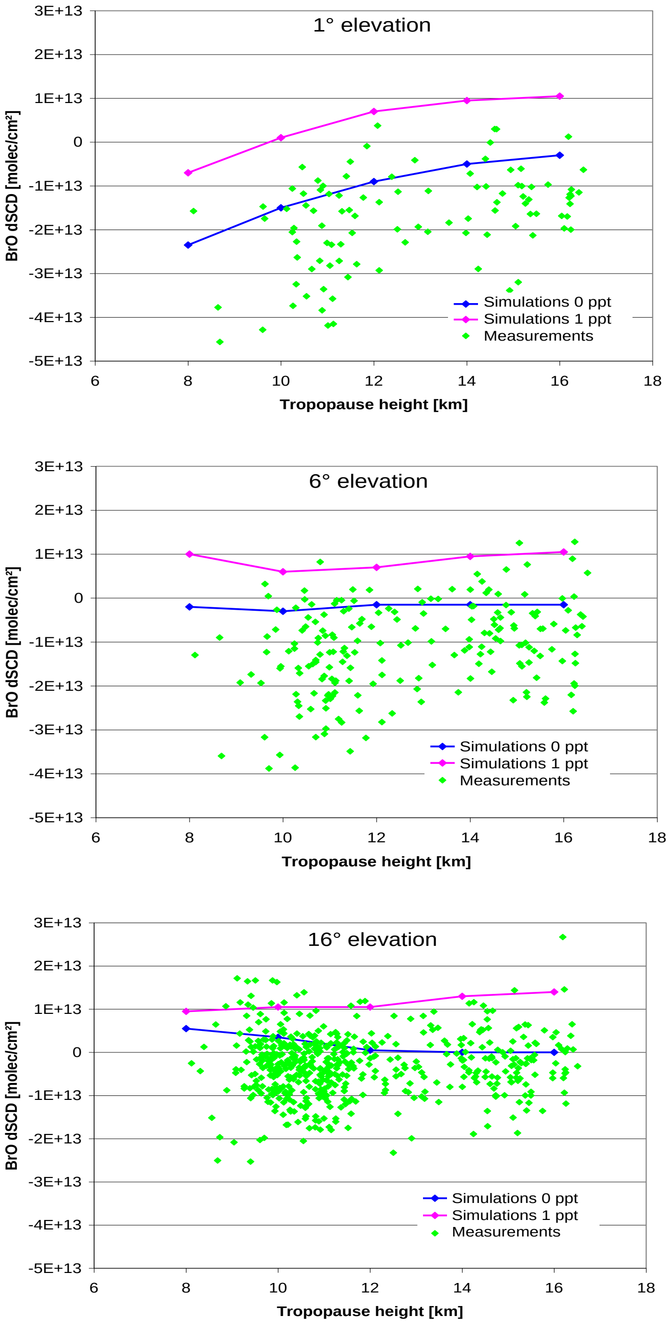

Fig. S31 Comparison of measured and simulated BrO dSCDs as function of the tropopause height for clear sky conditions. The blue and magenta lines represent simulation results for 1 ppt and 0 ppt BrO in the troposphere, respectively.

References

Bauer, R., Rozanov, A., McLinden, C. A., Gordley, L. L., Lotz, W., Russell Iii, J. M., Walker, K. A., Zawodny, J. M., Ladstätter-Weißenmayer, A., Bovensmann, H., and Burrows, J. P.: Validation of SCIAMACHY limb NO_2 profiles using solar occultation measurements, Atmos. Meas. Tech., 5, 1059-1084, 10.5194/amt-5-1059-2012, 2012.

Bogumil, K., Orphal, J., Homann, T., Voigt, S., Spietz, P., Fleischmann, O. C., Vogel, A., Hartmann, M., Bovensmann, H., Frerik, J., and Burrows, J. P.: Measurements of molecular absorption spectra with the SCIAMACHY Pre-Flight model: Instrument characterization and reference data for atmospheric remote-sensing in the 230–2380 nm region, J. Photochem. Photobiol. A., 157, 167–184, 2003.

Dorf, M., Butz, A., Camy-Peyret, C., Chipperfield, M. P., Kritten, L., and Pfeilsticker, K.: Bromine in the tropical troposphere and stratosphere as derived from balloon-borne BrO observations, Atmos. Chem. Phys., 8, 7265-7271, 10.5194/acp-8-7265-2008, 2008.

Lampel, J., Zielcke, J., Schmitt, S., Pöhler, D., Frieß, U., Platt, U., and Wagner, T.: Detection of O4 absorption around 328 and 419 nm in measured atmospheric absorption spectra, Atmos. Chem. Phys., 18, 1671-1683, 10.5194/acp-18-1671-2018, 2018.

Meller, R., and Moortgat, G. K.: Temperature dependence of the absorption cross sections of formaldehyde between 223 and 323 K in the wavelength range 225–375 nm, J. Geophys. Res., 105, 7089–7101, 2000.

Thalman, R., and Volkamer, R.: Temperature dependent absorption cross-sections of O2 –O2 collision pairs between 340 and 630 nm and at atmospherically relevant pressure, Phys. Chem. Chem. Phys., 15, 15371, 2013.

Vandaele, A. C., Hermans, C., Fally, S., Carleer, M., Colin, R., Mérienne, M.-F., Jenouvrier, A., and Coquart, B.: High-resolution Fourier transform measurement of the NO2 visible and near-infrared absorption cross sections: Temperature and pressure effects, Journal of Geophysical Research: Atmospheres, 107, ACH 3-1-ACH 3-12, 10.1029/2001jd000971, 2002.

Wilmouth, D. M., Hanisco, T. F., Donahue, N. M., and Anderson, J. G.: Fourier transform ultraviolet spectroscopy of the A2Π3/2–X2Π3/2 transition of BrO, J. Phys. Chem. A., 103, 8935–8945, 1999.